SAPIENZA
Università di Roma

PhD Programme in Life Sciences

XXXII Cycle

Collective properties of biological neuronal networks

Candidate
Silvia Ghirga

Supervisor
Prof. Alessandro Rosa

Tutor
Prof. Giancarlo Ruocco

Dr. Marco Leonetti

Coordinator
Prof. Marco Tripodi

Contents

Chapter 1

Introduction

1.1 Complex systems

Complex systems originate from the interaction of several elementary units that together appear to us as one unit displaying behavioral phenomena that are completely inexplicable by any conventional analysis of the systems' constituent parts. This is what is called a complex system. Science and nature are full of examples of complex system and evolution itself arises complexity. Indeed, hierarchical structures are prevalent in nature: molecules constituited by atoms, cells formed by subcellular organules, multicellular organism composed by cells[1]. Likewise, the most complex aspects of evolved multicellular organisms' brain emerge as consequence of the joint activity of billions of nerve cells. A primary challenge of neuroscience is to clear up how these cells, neurons, organized in the massive neural networks of the brain, communicate and dynamically regulate their connections to give rise to higher brain functions.

1.2 Neuronal networks

To study and understand the complex systems of neuronal networks, scientists can rely on an enormous amount of detailed knowledge, accumulated over the past one hundred years, about the structure

and function of neuronal cells. Neurons are excitable cell able to receive, integrate and transmit information through electro-chemical signal, called action potential. It is an all-or-none pulse, which consists in depolarization of the cell membrane followed by rapid hyperpolarization, then returning the membrane potential to the resting value. These changes in the membrane potential result from the sequential opening and closing of voltage-gated channel and are accompanied by influx and efflux of ionic currents (Na,Ca,K,Cl). Signal transmission between neuronal cells occurs by means of structures called synapses. Chemical and electrical synapses provide two distinct modes of direct communication between neurons. The first ones allow a wide variety of responses, varying in duration and intensity and represent a more complex behavior compared to the simple passive flow of current allowed from the electrical ones. One of the basic principle of neuroscience is that nerve cells do not connect randomly to each other in the formation of a network; but each cell forms a specific connection in particular points of contact with specific postsynaptic target cells and not with others. The strength of the connection is modulated by the activity of the network itself. So, if a synapse is activated the connection is strengthened (long term potentiation, LTP), otherwise it weakens (long term depression, LTD). These are the basis of the modern approach dedicated to the study of brain connectivity and are used for building models. The process of modelling aims to capture the essence of the complexity, abstracting the real system into a manageable size that is cognitively, mathematically and theoretically explainable. Models that simulate real-world complex systems are built to capture the dynamics and architecture of a system to predict the system's future behavior and to explain its past behavior. Such models help us to better understand and potentially fix system failures, such as those happening in disease processes inside human cells. Complex system can be mathematically represented by networks, defined by a set of nodes and links between pairs of nodes [2]. The complexity of the network arises as a combination of the number of nodes, the topology of connections and the behavior of single nodes (dynamic), distinguishing complex networks from randomly constructed networks (random) or regular networks. Neurons and synapse together consti-

tute the brain network. Depending on the spatial scale, we typically distinguish three types of neuronal units [2]: single neurons (order of μm), populations of neurons (hundreds or thousands of neurons in areas of the order of hundreds of μm to mm), brain areas (of the order of several mm). Modeling local microcircuits properties as well as large scale network properties is essential to understand how the brain works.

Among the connections, we can distinguish anatomical, functional and effective connections [3]. Anatomical connectivity is the set of physical or structural connections (such as electrical or chemical synapses) that connect neuronal units at a given instant. Anatomical connectivity is static at time scales ranging from seconds to minutes and dynamic from hours to days, for example during learning or development. Functional connectivity represents the emerging connections from a measure of statistical dependence between neuronal units. Different approaches used to measure the activity lead to different results in terms of the statistical estimation of functional connectivity. Then functional connections can also occur between anatomically unrelated regions. Functional connectivity is independent of time in the order of hundreds of ms and is not based on models in the sense that it measures a statistical dependence without explicit reference to causal effects. Effective connectivity, instead, describes the set of causal effects that one neural unit has on another. Unlike functional connectivity, it requires the specification of a causal model that includes structural parameters. The types of possible links are summarized in 1.1 with reference to the trivial case of three neural units.

1.3 Network Proprieties

Mathematically, networks are represented by graphs [3]. A graph is a set of n nodes, which represent neurons, and k links, which represent anatomical, functional or effective connections. If we distinguish the directionality of the connections, the graph is called direct, otherwise adirectional. The structure of a graph can be described by a squared matrix (called adjacency or connectivity) with a size equal to the number N of nodes. The elements a_{ij} of the matrix can be

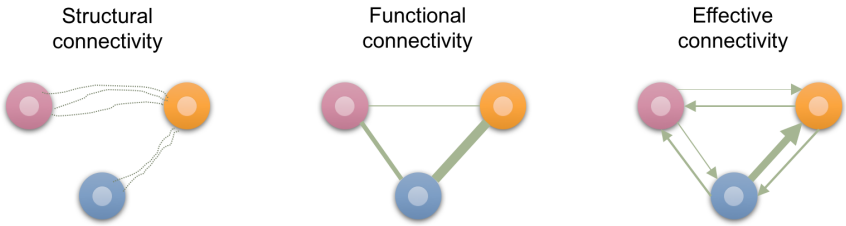

Figure 1.1: **Types of connectivity** Structural connectivity (due to physical connections), functional connectivity (due to statistical dependencies that do not imply causal connections and that is not directional) and effective connectivity (random and directional).

binary, indicating the presence (a_{ij}= 1) or the absence (a_{ij}= 0) of connections, or real, in the case in which the connections are weighed. The mathematical features of a graph are given by various parameters which give a simple and clear indication of the type of connectivity. Below we define most significant parameters.

Node degree is defined as the sum of incoming (afferent) and outgoing (efferent) connections: $k_i = \sum \epsilon N a_{ij}$. Depending on the degree distribution of the nodes, three different types of graphs can be distinguished:

Random graphs, in which the distribution of the degree of the nodes is binomial [4]: $p_k = \binom{N-1}{k} p^k * (1-p)^{N-1-k}$

Regular, ordered graphs characterized by a high segregation value. In this case, the distribution of node degrees is simply a constant: $p_k = c$.

Scale-invariant graphs, characterized by high-connection units, called hubs. Hubs are nodes with a degree at least equal to a standard deviation from the average grade of the network [5]. Because of this feature, hubs play a crucial role in network dynamics: if removed, they cause the loss of information. The degree distribution of the nodes is a power law: $p_k = k^{-\gamma}$, where γ is a characteristic exponent of the experimental sample, of order 1.

Clustering coefficient. The clustering coefficient of a node is the number of connections with the first neighbors with respect to the number of maximum possible connections: $C_i = \frac{n_i}{(k_i(k_i-1)/2)}$, where

C_i is the clustering coefficient of the i-th neuron, n_i is the number of connections between first neighbors of the neuron, k_i the number of its connections and $k_i(k_i - 1)/2)$ the maximum number of possible connections. Calculating the average value of the clustering coefficients of all the neurons in the network, we obtain the average value of the clustering coefficient, which quantifies the level of segregation of the network. Random networks have low clustering coefficient values whereas complex networks have high clustering values.

Path length. A path is defined as an ordered sequence of distinct connections and nodes that bind a node i to a node j. In a given path no connection or node is visited two or more times. The length of a path is equal to the number of connections necessary to go from node i to node j. The distance between a node i and a node j is defined as the length of the shortest path. $d_{ij} = \sum$. Random and complex networks have small distances while regular lattices have long distances. Distance is inversely proportional to the network's efficiency in transporting information.

Connection density. Is defined as the ratio between the number of connections in a network and the total number of all possible connections. It is directly connected to the energy cost of a network in transferring information.

We have seen the characteristics of random and regular networks. Complex neuronal networks have intermediate properties: an asymmetric distribution of node degrees, a high value of the clustering coefficient, the presence of hubs and modularity. Furthermore, complex networks tend to be characterized by high clustering values combined with small values of medium distances (small - world). This type of structure causes all the nodes of the system to be linked together by a relatively small number of connections, even though most nodes have few connections. The small - world organization is intermediate between that of a random network where the small average distance is associated with a low clustering value, and that of a regular reticular network, in which the high clustering value is connected with a high average distance. To characterize the small-worlds, various measures have been proposed, based on the idea of comparing the value of the clutering coefficient and the average path with respect to those of an

equivalent network (with the same number of nodes and connections) random. Humphries et al [6] proposed the coefficient σ defined as: $\sigma = \frac{C/C_{rand}}{L/L_{rand}}$ The classification condition of a network as small-world is that $C \ll C_{rand}$ e $L \approx L_{rand}$ or $\sigma > 1$.

1.4 Recording neuronal activity

Recording measurements of neuronal activity is fundamental to understand and model neuronal circuits functioning. The complexity of the brain requires all different modeling strategies to deal with both the complexity of its physiology and biology. Modeling local micro-circuits properties as well as large scale network properties are crucial to understand how the brain works. Several experimental techniques are nowadays available to monitor directly or indirectly electrical neuronal activity on different spatial scale. Since two centuries, electrical methods have been used to control and stimulate electrical activity in neurons [7] [8]. Patch Clamp is an electrophysiological technique, developed by Neher and Sakmann between the 70s and 80s, to measure electric current across single ionic channel or whole cell membrane [9] [10]. This is one of the most recognized tool to study functionality at the scale of single neurons. On the other hand, multiple electrodes can be applied to the scalp of the subject to measure electrical activity of many neurons from different brain areas (electroencephalography, EEG). Other techniques such as magnetoencephalography (MEG), functional magnetic resonance (fMRI) and positron emission tomography (PET) allow indirect detection of large-scale neuronal activity by measuring correlated quantities (magnetic fields, blood oxygenation level, variation of blood flow). Specific functionalites of various cortical regions have been explained within these tools. Not only the areas dedicated to sensory processes, but also those that perform high-level perceptual analysis of faces, places, bodies, words. Similar clues also concern the localization of language, musical skills and some aspects of mathematical skills [11]. Anyway, it still remains unanswered which are the neuronal circuits that allow each area to perform its particular function and the connectivity mechanisms that allow the development of these cortical regions. While is quite simple

to study neuronal functioning at single-cell level or brain-areas scale using standard techniques, it becomes challenging when it comes to neuronal circuits. Indeed, to study the activity of populations of neurons it would be require collecting, at the same time, individual signals from hundreds of neurons with sufficient resolution. Patch Clamp techniques lacks the possibility to control activity of a big number of neurons simultaneously. Devices such as Multi Electrode Array (MEA) attempt to remedy this problem [12]. MEA consist in multiple (tens to thousands) microscopic electrodes through which neural activity is recorded and stimulated. Anyway, commercial chips have a limited number of electrodes and electrode size (hundreds of microns) limits the measurements to a population response. Customs devices with elevated number of smaller electrodes (tens of micron) are emerging and provide better spatial resolution but analysis of the recorded data becomes more complex [13]. Beside the generally poor spatial specificity, electrical stimulation and recording suffer the electrical interference from the environment, intrinsic damage caused by direct contact with the electrodes and the presence of high-frequency artifacts associated with the stimulation signal. To overcome these limitations, over the past decades, novel techniques based on optical recordings were designed [14]. Calcium imaging with fluorescent indicators provides an optical approach to monitor action-potential-evoked calcium transients. Since the introduction of calcium imaging to monitor neuronal activity over wide field with single-cell resolution, optical imaging methods have revolutionized neuroscience.

Light has the advantage of being non-invasive and spatio-temporally controllable with high precision. In addition, no direct contact is necessary between the stimulating source and the tissue, preventing cells damage [15] [16]. Optical imaging methods have represented a great stride in neuroscience by enabling systematic recordings of neuronal circuits in living animal. Anyway there are serval physical problems that different microscopes are made to solve: deliver photons effectively to the sample, minimize the dose of excitation light, collect emitted photons efficiently and perform measurements with high temporal and spatial resolution in as large and deep a territory as possible, all while preserving good signal-to-noise ratio (SNR) [17]. This is

technically challenging to be achieved *in vivo*, dissociated and *in vitro* cultured neurons may serve as a more accessible model sample to understand the insights of network dynamics. Indeed, transparent *in vitro* 2-D cultures present the advantage of being observable by traditional wide-field microscopes. The basic wide-field fluorescence microscope illuminates the sample over an extended area (mm size) and captures the emitted fluorescence of single cells with a camera, and imaging speed is limited only by camera frame rate, which approaches 500 frames per second (fps) for scientific complementary metal oxide semiconductor (sCMOS) cameras.

1.5 *In vitro* model

Although *in vivo* system represents the ideal framework to study functional brain activity and, as we have seen, in the past decades significant result have been achieved, they suffer two main limits. The first one, as we anticipated in the previous paragraph, is related to the resolution of the experimental techniques available *in vivo*. Neural circuits are composed of hundreds of thousands of neurons that are interconnected in a highly distributed manner. To study emergent functional properties is required to record the activity of many, or most, neurons in a circuit in order to capture the functional properties built by the entire population. Access to such data in living animals is a primary goal of neuroscience but is still technically challenging to be achieved and requires complex data analysis algorithms [18], [19]. For this reason, primary neurons isolated from animal brain and *in vitro* cultured, represent a suitable model to deeply investigate neuronal network dynamics. Transparent *in vitro* 2-D cultures benefit from traditional wide-field microscopes, which offers high spatio-temporal resolution over a large area, ideal for mapping neuronal activity. The other limit concerns the impossibility to manipulate network and external parameters, such as excitatory/inhibitory balance, temperature or surrounding ionic concentration, in living subject, while *in vitro* environment lends itself to be easily shaped. In the past decades, general physical principles were elucidated within this framework, such as theta rhythm [20], synapse dynamics [21] or the emergence of

small-world architecture [22] [23] and coherent activity [24]. Cultures ability to mimic the behavior *in vivo* is most exemplified by the fact that primary cortical cultures can also exhibit the default activity pattern that living cortex display when virtually isolated, thus in the absence of external stimulus (such as during sleep or anesthesia) [25, 26, 27].

1.6 Cortical Slow Oscillations

The mammalian cortex is an intricate network of synaptic connections: most of excitatory synapses onto cortical excitatory neurons come from other cortical excitatory neurons [28, 29, 30]. This recurrent connectivity allows cortical neurons to generate patterned network activity, even when the cortex is virtually disconnected. Indeed, during quiescent periods, such as sleep or anesthesia, the entire neocortex spontaneously undergoes slow, synchronized transitions between sustained periods of synaptic activity (Up states) and relative periods of silence (Down states). This alternation ($<$1 Hz) between Up and Down states are called slow oscillations (SO) [25, 26, 27, 31]. The occurrence of SO during slow-wave sleep and ketamine anesthesia has been observed since the early times of electroencephalography [32] but this oscillations were at first characterized only decades later in the neocortex of the cat [33]. Since then, great strides have been made in elucidating the cellular and network mechanisms behind this widespread phenomenon, but several mechanistic features of the slow oscillation, however, remain to be explored. One of the main characteristic of SO is their multiscalarity: SO show similar features whether they are observed in the intact cortex of a sleeping human, in a small piece of cortex on a plate and even in random cortical networks ex vivo. This multiscale property originates from the fact that SO rely mostly on local connectivity and not on long-range connectivity. The persistence of SO also in large cortical network isolated from the living brain is the main argumentation demonstrating that the alternation between metastable cortical states is the default cortical activity regime. Even if such bi-stable pattern is quite resilient to changes, spatial and temporal properties of the SO can be modulated

by modifying network or environmental proprieties, such as excitatory/inhibitory balance [34], temperature [35], extracellular potassium [36], etc. These physiological parameters shape SO and, in the same way, the shape of cortical SO gave information about the state of the underlying network. When there are pathologies that disturb cortical circuits, we can expect that they will be reflected in the disruption of slow waves. Following this principle, recordings from a pathological network may reveal alterations in the SO proprieties. Several recent works have shed light on the modification of SO features in animal models of neurological disorders, with a particular attention on Alzheimer's disease [37, 38]. Indeed, the phenomenon of SO is related to the consolidation of memory, if slow wave sleep periods are disturbed, cognitive functions such as attention and memory can be negatively affected.

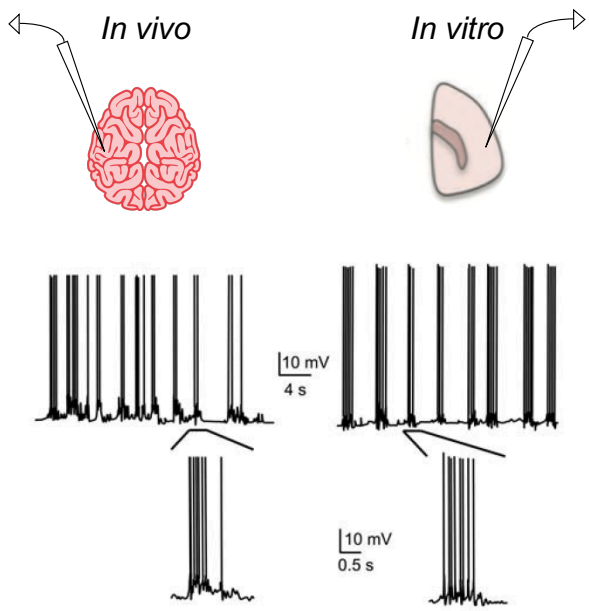

Figure 1.2: **Cortical Slow Oscillations.** Generation of the slow oscillations *in vivo* (intracellular recording of primary visual cortex of anesthetized cat) and *in vitro* (intracellular recording of slices of ferret visual cortex). Adapted from *Sanchez-Vives, M. V., & McCormick, D. A. (2000). Nature neuroscience.*

Thus, slow waves, universal across species and patients, detectable from whole living cortex as well as from single neurons on a dish, represent a unifying paradigm to study emergent properties of the collective dynamics in cortical module: from inter-neuronal connectivity to slow-wave propagation, providing an easy probe to understand basic functioning of cortical circuits and their pathological alteration.

1.7 Alzheimer disease model: 3xTg mouse strain

So far, we have seen how the cortical networks spontaneously fall into a bi-stable rhythm or SO, how this rhythm is robust to perturbations, and how alterations in SO parameters reveal abnormalities in the underlying network [37, 38]. On this basis, recent studies has focused on the characterization of SO in animal models of neurological disorders. Of particular interest are previous works aimed to characterize cortical emergent rhythms in transgenic mouse model of Alzheimer's disease. Alzheimer's disease (AD) is a primary neurodegenerative disorder that causes a progressive impairment of memory and other cognitive functions, and represents the leading cause of dementia among the elderly. The principal neuropathological hallmarks of AD are the abnormal accumulation of the amyloid-β (Aβ) peptide forming Aβ plaques, the hyperphosphorylation of the microtubule associated protein tau, known as neurofibrillary tangles, the loss of neurites and synapses, and cellular death at advanced stages of the disease. These changes in the brain are accompanied to neuronal activity dysfunction such as hyperexcitability [39], long term potentiation deficit [40] and altered connectivity. Graph theoretical analysis applied to matrices of functional connectivity of beta band–filtered electroencephalography (EEG) channels on human patients demonstrates that AD is characterized by a loss of small-world network characteristics [41]. Aβ-induced dysfunction of inhibitory interneurons likely increases synchrony among excitatory principal cells and contributes to the destabilization of neuronal networks [42]. To further investigate these alterations with high resolution technique we required a good *in vitro*

model of AD. Most AD cases are sporadic and result from multiple etiologic factors, including environmental, genetic, and metabolic factors, whereas familiar AD is caused by mutations in the presenilins or amyloid-β (Aβ) precursor protein (APP) genes. As advances were made in the field of genetics, scientists became increasingly adept at manipulating genome of mice. The 1980s saw an explosion in this technology with the advent of transgenic mice carrying additional genetic material. A commonly used animal model for AD is the 3xTg-AD triple transgenic mouse model, which harbors mutated presenilin 1, APP, and tau genes and thus represents a model of familiar AD. 3xTg-AD develops Aβ and tau pathology in a progressive, temporal- and region-specific manner that resembles that in human AD brain. Cognitive impairment is known to exacerbate in an age-dependent manner in 3xTg-AD mice [43]. Long-term retention deficits start to manifest at the age of 4–5 months, and short-term memory is affected by the age of 6–7 months. When these mice are 18-month old, they are unable to learn the platform location in the water maze, indicating inability to encode and/or remember spatial information, a characteristic of cognitive failure relative to hippocampal impairment [44]. These neuropathological and behavioral AD-like hallmarks are likely to be accompanied by disturbances in cortical network activity. Patricia Castano-Prat et al. [37] compared the Up and Down states of the spontaneously generated cortical SO, between the 3xTg-AD mouse model of AD and control mice at different ages. This study, performed *in vivo* during ketamine-induced anesthesia, reveals that 3xTg-AD mice presented alterations in the emergent cortical activity with respect to controls, and the electrophysiological phenotype of 3xTg-AD animals changed with age in a different manner compared to that of control animals. Vale et. al [45] showed that an increased expression of amyloid precursor protein, amyloid-β and tau occur also in primary cortical neurons derived from 3xTg-AD embryo. Thus, 3xTg-AD *in vitro* primary cortical cultures provide an ideal experimental framework to deeper investigate the effects of neuropathological AD-like hallmarks on network activity. On one side, they allow to study the collective phenomenon of the slow oscillations, spontaneously expressed by the isolated cortical neurons, and how SO characteristics

are modulated by changing physiological parameters. On the other hand, *in vitro* cultures enable to study neuronal activity with highly precise spatio-temporal resolutions (μm-ms) exploiting imaging techniques. The ability to detect signals from hundreds of single neurons simultaneously allow to infer the microscopic dynamical properties of the network in different conditions.

1.8 Aim

The aim of this thesis was to combine a custom-made high-resolution wide-field calcium imaging setup and personalized data analysis algorithms, inorder to investigate cortical emergent rhythms and provide insights into the microscopic network mechanisms underlying associated network activity alterations in 3xTg-AD strain derived cortical network. We could rely on the use of a homemade fluorescence microscope optimized for this purpose: the full-field signal is captured with a sCMOS camera which allows for high-speed measurements (200 frames/s) and a low magnification objective (5x) was chosen to observe large areas ($> 1mm^2$) with high spatial resolution (1 pixel 2 μ m). Furthermore, a LED light source was chosen to excite the calcium sensitive dye loaded in the cells. The use of a low-power LED light minimized the effects of fluorophores photo-bleaching and prevented the cells damage, while preserving a good SNR. Data analysis was performed using a custom MATLAB software that we develop to process fluorescence data. In short, our algorithm automatically identifies neurons centroids, extracts individual neuronal signal, detects the occurrence of spike-associated calcium events and reconstructs the signal through a double fitting method. This procedure allowed revealing neuronal activity of large cortical areas with near millisecond precision, which in turn informed about network connectivity. Indeed, functional connectivity of the network can be evaluated from the binary traces through a previously described algorithm based on generalized transfer entropy (TE) method [46, 47, 48]. TE measures the amount of directed information between each pair of neurons. By definition, TE is directional and dynamic, being asymmetric and defined on transition probabilities and importantly data-driven TE approach

used is model-independent. With this procedure allowed us reconstruct network functional connectivity and thus to evaluate network proprieties. The purposed analysis will provide massive information about the synchronization of cortical activity and the anomalies that can occur because of environmental modification or specific pathology. The final intent of this work is to deepening the microscopic proprieties of cortical network and their alteration in *in vitro* model of Alzheimer's disease. Thus we:

- designed and built the custom-made fluorescence microscope to perform wide field calcium imaging experiments;
- isolated and cultured *in vitro* cortical neurons derived both from 3xTg-AD mouse strain and control animals;
- measured spontaneous calcium activity of *in vitro* cortical networks, at different stage and under different conditions;
- developed an automated and personalized algorithm to analyze fluorescence data and extract single neuron activation with near millisecond precision;
- analyzed properties of the collective slow oscillations and signal propagation;
- used a generalized transfer entropy method to infer network connectivity and study network features;
- assessed the effects of the neurodegenerative disease.

Chapter 2

Materials and Methods

2.1 *In vitro* primary cortical cultures

In vitro neuronal cultures have been recognized as a successful model system of neuronal activity. As well as lending themselves to be easily manipulated (by modifying environmental or network proprieties), they benefit from high-resolution imaging technique available to monitor behavior of collective dynamics.

2.1.1 Animals

Procedures using laboratory animals were in accordance with the Italian and European guidelines and were approved by the Italian Ministry of Health (n. 253/2016-PR) in accordance with the guidelines on the ethical use of animals from the European Communities Council Directive of September 20, 2010 (2010/63/UE). All efforts were made to minimize suffering and number of animals used.

2.1.2 Cultures preparation from early post-natal mice cortex

Primary neuronal cultures were prepared from the brain of 0-2-d-old mice using culturing protocols previously described [49], Fig.2.1. In brief, after removal of the meninges from the whole brain, cerebral

cortices of both hemispheres were isolated and digested in 0.125 % trypsin for 30 min at $37°C$ followed by 5 min DNase incubation 0.3 mg/ml at RT. Cells were mechanically dissociated with a fire-polished Pasteur pipette and plated at a density of 2.5 X 10^5 on poly-L-lysine-coated glass coverslips. Neurons were maintained in serum-free Neurobasal supplemented with 2% B27, 1% L-Glutamine and 1% Penicillin-Streptomycin solution. Cells were cultured in controlled environment for 7-30 days in vitro (DIV), with a humidified atmosphere containing $5\%CO_2$ at $37°C$. 2 days after plating cytosine arabinoside (araC) were added at a final concentration of 1.5 μM to limit the proliferation of dividing non-neuronal cells. With this method we obtained 80-90% neurons, 8-15% astrocytes, and 2-5% microglia, as determined with β-tubulin III, glial fibrillary acidic protein (GFAP), and isolectin IB4 staining, Fig.2.1. Neurons in culture grew and developed processes within hours, and by DIV 7 formed an active network with sustained spontaneous activity. Measurements of

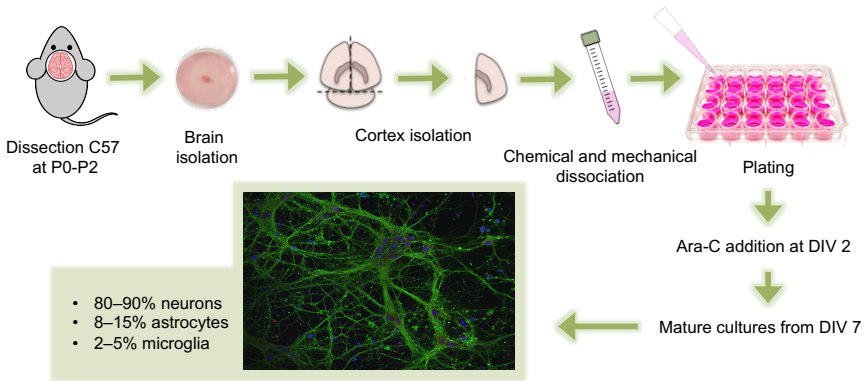

Figure 2.1: **Culturing pyramidal neurons from the early post natal mouse cortex.** Mouse cortex were isolated, chemically and mechanically dissociated, and cells were plated on 24-well multiwell. Addition of ara-c limit the proliferation of non neuronal cells. We obtained culters with 80-90% neurons, 8-15% astrocytes, and 2-5% microglia, as determined with β-tubulin III, glial fibrillary acidic protein (GFAP), and isolectin IB4 staining. Neurons in culture display rich spontaneous activity by DIV-7.

neuronal calcium activity were carried out at DIV 7-30 using custom-made fluorescence microscope described in the next section 2.2. Prior the experiment, culture medium was replaced with a normal external solution (NES) containing: 140 mM NaCl, 2.5 mM KCl, 2 mM $CaCl_2$, 2 mM $MgCl_2$, 10 mM HEPES-NaOH and 10 mM glucose (pH =7.3 with NaOH; osmolarity 300 mOsm). Cultures were incubated for 30 minutes in recording solution with $5\mu M$ concentration of the calcium-sensitive dye Fluo-4-AM (ThermoFisher), then were washed off Fluo-4 and placed on the recording incubator mounted on the microscope. All experiments were performed at 32 °C, except when expressly stated.

2.1.3 Small-size cultures

In order to control simultaneously the dynamics of the whole culture, thus visualizing the whole culture in the field of view of the camera, we create small, millimeter-sized cultures. Cortical neurons were plated on 12 mm glass coverslips (CS-12R15, Mutichannel Systems) that contained a pierced PDMS mold, as illustrated in Fig.2.2. Prior to plating, glasses were washed in 70% ethanol and flamed. Several 12 mm diameter layers of PDMS 1 mm thick were prepared and subsequently pierced with biopsy punchers (rapid core, Welltech) of diameters in the range 1.5-6 mm. Each pierced PDMS mold typically contained 4 to 8 cavities, either circular or quasi–rectangular by overlapping consecutive pierced areas. The PDMS molds were then attached to the glasses and the combined structure were placed in 15 mm diameter culture wells for neuronal plating and maintenance. The

PDMS was gently removed before measuring, and we did not detect any substantial damage in the network after PDMS removal. Measurements from a portion of the culture can lead to record neuronal activation that are due to external unviewed input (neurons outside the field of view). This can cause the identification of spurious and non-real correlations between neurons, which negatively affect connectivity inference. Avoiding this effect, small size cultures allowed a more precise reconstruction of the network. Additionally, measures

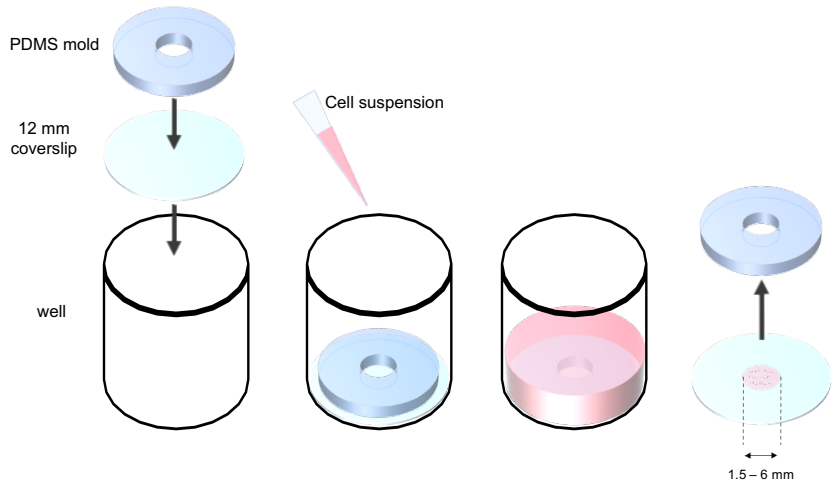

Figure 2.2: **Millimeter-size cultures.** Small neuronal cultures were obtained by plating cells on 12-mm coverslip covered with 1 mm layer of pierced PDMS. The PDMS mold was gently removed before recording.

from cultures with different size allowed to explore how this parameter influence network activity and functional connectivity development.

2.1.4 Physiological parameters

Excitatory-Inhibitory ballance. Sufficiently mature neuronal cultures (above DIV 7) contain both excitatory and inhibitory neurons. To study the contribution of the inhibitory sub–network in the spontaneous activity, data was first recorded with both excitatory and inhibitory connections active (E+I networks). Next, the culture was treated with 20 μM bicuculline methiodide (1030/50, Biotech), a GABA receptor antagonist, to completely block inhibition, and the activity of the excitatory–only culture (E network) was measured again. Bicuculline was applied to the culture 5 min before the actual recording of activity for the drug to take effect.
Excitability. In order to increase calcium events frequency in culture with poor spontaneous activity, some of the experiments were carried out after the addition of 4-Aminopyridine (4-AP, 2 mM, 275875, Sigma-Aldrich) which blocks voltage-activated K^+ channels. 4-AP is

a potent convulsant, generally used to cause epileptiform activity in *in vitro* preparations [50].

TRPV4 blockage. In the work described in chapter 3 some experiments were repeated after the addition of 5 μM concentration of RN1734 (R0658, Sigma-Aldrich), a selective antagonist of thermosensitive transient receptor potential vanilloid channel TRPV4 [51] [52] [53].

Firing inhibition. To detect spontaneous calcium oscillations in the absence of spike driven calcium entry, additional experiments were done following the blockage of electrical activity through 1 μM tetrodotoxin (TTX, 1078, Tocris) administration. It's a neurotoxin which inhibits the firing of action potentials by binding the voltage-gated sodium channels on cell membranes and blocking the passage of sodium ions into the neuron.

2.2 Calcium imaging setup

Transparent *in vitro* 2-D cultures present the advantage of being observable by traditional wide-field microscopes. This technology offers high spatio-temporal resolution over a large area, ideal for mapping neuronal activity. In this section, we report about the schematics of the homemade fluorescence microscope optimized for this purpose: the wide-field signal was captured with a sCMOS camera (ORCA-Flash4.0 V2, Hamamatsu, pixel size = 6.5 μM) which allowed for high-speed readout (up to 1000 frames/s), a low magnification and relatively high numerical aperture objective (High-Res 5X, 0.225 NA, 28-20-44, Optem) was chosen to observe large areas ($>$1 mm^2) with single cell resolution. We combined the objective with an eyepiece with shortest focal length (LA-1986-A, f=125 mm, Thorlabs) to reduce the overall magnification from 5X to $\sim$3X (pixel size $\sim$ 2 μm). To minimizes the effects of fluorophores photo-bleaching and prevents the cells damage, while preserving a good SNR, we used a low power LED light source centered at 490 nm (M490L3, ThorLabs) to excite the calcium sensitive dye Fluo4-AM loaded in the cells. In detail: the LED light, filtered with a band pass filter (FB480-10, Thorlabs) was

focused on the sample to excite the fluorescent molecules bound to calcium ions. The emission is collected by the objective, filtered by a dichroic beamsplitter (FF495-Di03-25x36, Semrock) that reflects all the spectral region above 495 nm, and imaged on the display of the computer through the camera after being further cleaned by a long-pass filter which cut wavelengths below 500 nm (FEL0500, Thorlabs). Optical setup is also equipped with a temperature controller (TC-324B, Warner Instruments), which enables to regulate temperature and maintain it stable during the recording, and a perfusion-aspiration system that allow the release of chemical compounds to the specimen. The system configuration is illustrated in Fig.2.3. LED light and camera recording are controlled by a custom MATLAB code through a Data AcQuisition (DAQ) board. Images were acquired with a speed in the range of 1 - 200 frames per second (fps) and a pizel size of 1.8 μm/pixel. The recording speed was adjusted in each experiment to balance image quality, minimum photo–damage to the cells and sufficient temporal resolution. The size of the images was manually set to fit the requested acquisition speed. The maximum image size that we could set was 1600x1600 pixels, i.e. 3.5x3.5 mm ^{2} at the lowest resolution and acquisition speed (33.33 fps). At 200 fps, for instance, the maximum image size was 200x200 pixels, corresponding to 400x400 μ m^2. The number of neurons monitored depended on the actual size of the culture and the recording settings, but all experiments contained from 100 to 1000 neurons.

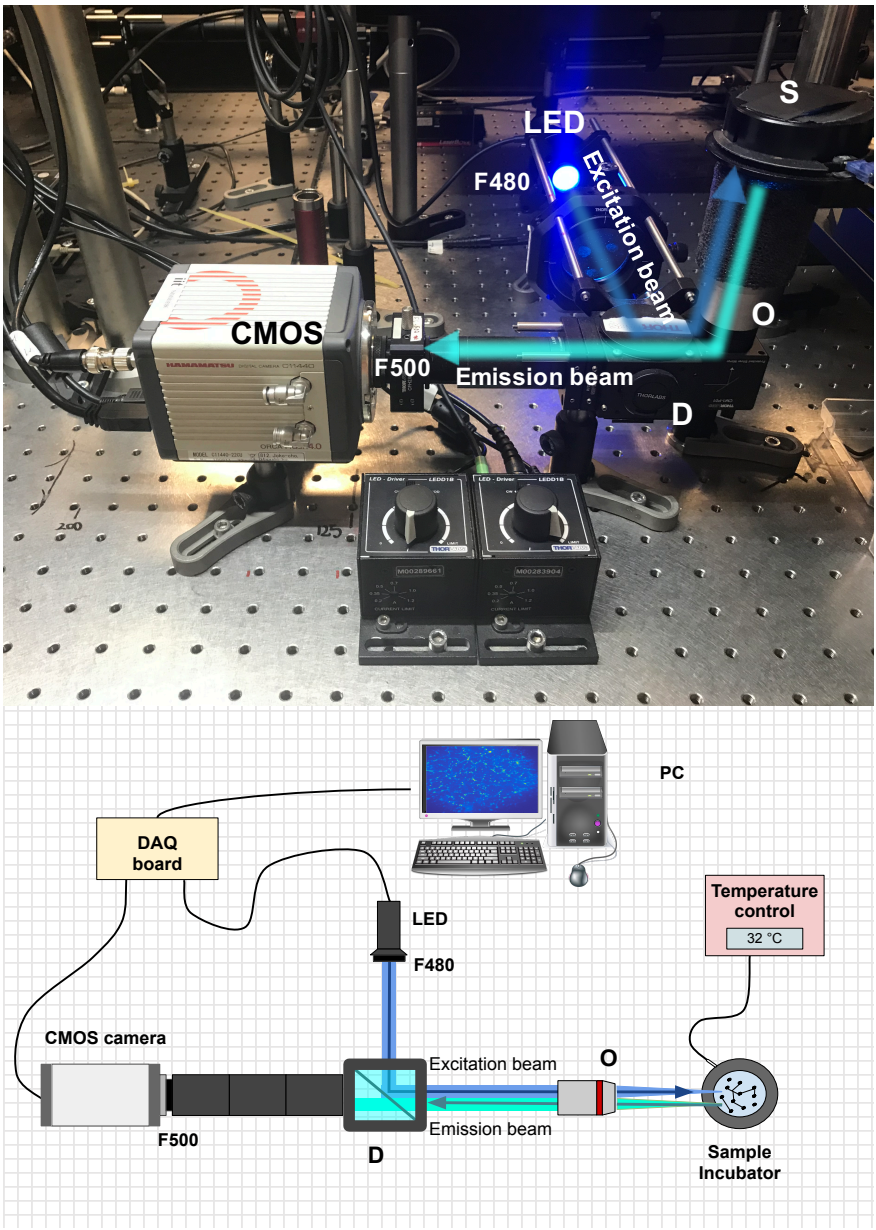

Figure 2.3: **Optical setup.** LED light source centered at 490 nm was focused on the sample (**S**) loaded with Fluo-4 and excited the fluorescent molecules bound to calcium ions. The emission is selected with a filter and collected by the objective (**O**) and imaged on the display of the computer through a CMOS camera

2.3 Data analysis

The advantage of our experimental setup is the possibility to access statistical proprieties of large biological networks because of the wide field calcium imaging of the cultures. However, to extract the information from images requires an extended analysis. In this section we will explain the analysis methods used in this work, which can be divided in three main parts: neurons recognition, calcium events detection, SO analysis and connectivity inference. All data processing was performed through numeric codes implemented in MATLAB environment, except for Events Coincidence calculation implemented in Pyton.

2.3.1 Neurons recognition and spike inference

At the end of each experiment, the recorded image sequences were collected and saved as three-dimensional matrix. The first step of data processing consists in the localization of the cells body position on the images. Neurons centroids were identified by analyzing the cumulative difference of the signal between the various frames of the time series. The obtained matrix is analyzed in the frequency domain via two-dimensional Fourier transform and suitably filtered to eliminate high-frequency noisy components; then the local maxima of the matrix are selected Fig.2.4. Once established cells positions (100 – 1000 for each area scanned, depending on the size of the area), their fluorescence signal as function of time, mediated within a distance comparable to soma radius ($\sim$ 15 microns), were collected and taken as an indicator of intracellular calcium at the level of neuronal soma. The raw traces of the neurons extracted from the t-stack were baseline-corrected and normalized as $\triangle F/F_0$. Traces were then filtered using a previously described [54] modified Perona-Malik filter, an edge-enhancing denoising algorithm that performs smoothing within slow varying regions and prevents smoothing across fast varying regions Fig.2.5 (preserving fast varying fluctuation events associated with the electrophysiological activity of the neurons). On the filtered traces, a putative event is detected when a series of conditions are satisfied:

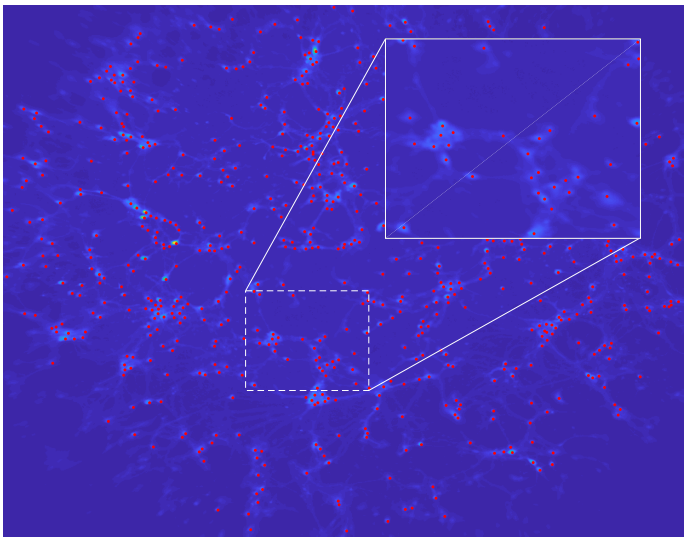

Figure 2.4: **Neurons detection.** Data were analyzed in the frequency domain *via* two-dimensional Fourier transform and suitably filtered to eliminate high-frequency noisy components; neurons position were identified as the local maxima of the matrix.

at the onset the fluorescence intensity and the slope of the trace show an increase; at the offset the slope of the trace decreases and a certain time interval occurs within the onset and the offset [54] Fig.2.5. This operation gave a first indication about the onset time of each events, which were used as starting point for a fitting procedure based on a previously described peeling algorithm [55]. The algorithm assumes that there exists an elementary calcium transient characteristic of a single action potential and that the calcium transients add up in a linear fashion. Each putative transient was fitted in two-step with a model function composed of a single-exponential rise and a single-exponential decay Fig.2.5.

$$I(t) = a * exp^{-\frac{t-t_0}{\tau_{on}}} * (1 - exp^{-\frac{t-t_0}{\tau_{off}}}) \tag{2.1}$$

In the first step, we fitted the onset to determine the start of the event t_0 and the onset time constant τ_{on}. Then we fitted the entire calcium transient to obtain estimates of amplitudes a and time constants the decay components τ_{off}. The fitted calcium signal is then subtracted from the trace and we proceed by iteration until all the calcium transients have been eliminated from the time series and for each neuron the onset time of each events t_0, with near ms precision, and the relative characteristics $(\tau_{on}, \tau_{off}, a)$ were saved. This procedure enable the reconstruction of complex spike trains from fluorescence traces. The inference of the events onset with oversampling precision is crucial for a correct reconstruction of casual interaction among neurons.

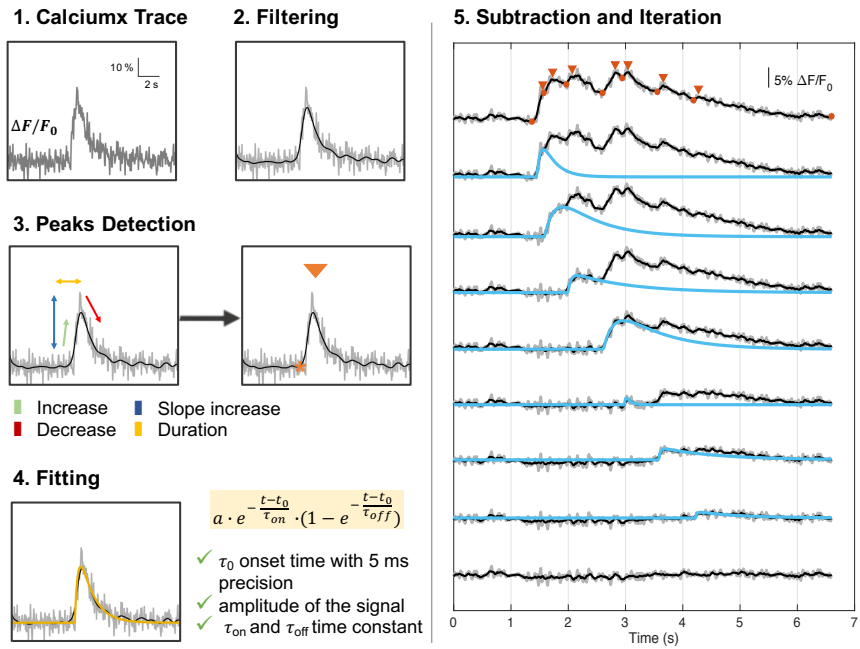

Figure 2.5: **Events detection from calcium traces.** Schematics explanation of peaks detection protocol: on baseline corrected (1) and filtered (2) calcium trace, a putative peak was identified when a series of condition were full-filled (3) and then fitted in a two step procedure to obtain real onset time and relative features (4).The fitted calcium signal is then subtracted from the trace and we proceed by iteration (5) until all the calcium transients have been eliminated from the time series.

2.3.2 Slow Oscillations analysis

As explained in section 1.6, cortical networks spontaneously undergo simultaneous oscillation (SO) between periods of collective activity (Up states) and periods of relative silence (Down states). To characterize this emergent activity regimes in early mature cultures under different condition, the averaged signal of the whole network served as an indirect but reliable indicator of the network collective dynamics. From the averaged fluorescent signal we extracted and compared several parameters of the SO: frequency of oscillation, up

state duration, down state duration, slope of down-to-up state transition, slope of up-to-down state transition, relative firing rate, CV of the up state duration, CV of the down state duration, and CV of the up state–down state cycle. On the cumulative traces, events detection was performed as described for single neurons traces. Then, Up states were then identified when a series of events occurs consecutively with inter-event-intervals below 1 second. Time windows between different Up states were assessed as Down states, Fig.2.6. The frequency of the SO was calculated as the inverse of the duration of the whole Up-Down cycle. We evaluated mean Up and Down duration for each recording. To determine the characteristic frequency of the Up state we mediated the inverse of the inter-events intervals of single neurons per Up state. The CV was previously defined as the fraction between the standard deviation and the mean value of the durations of Up and Down states and of the whole Up-Down cycles singled out for each recording, respectively [25].

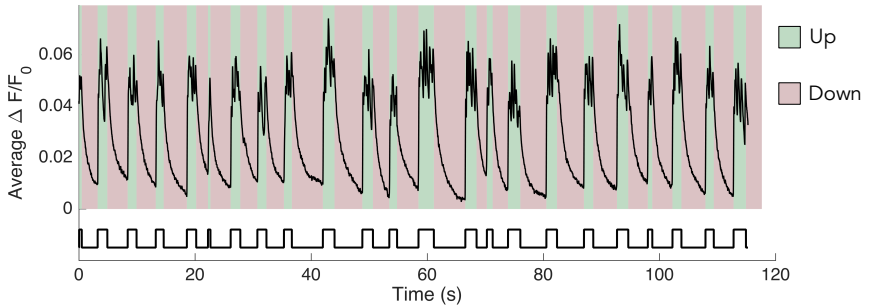

Figure 2.6: **Up and Down states identification.** Once detected events occurrence on the averaged fluorescence signal, Up states were then identified looking for consecutive events occurring with an inter-event-intervals smaller then 1 s. Down states results between the end of an Up state and the beginning of the following one.

2.3.3 Signal Propagation

The propagation of the slow oscillations could occur in either direction, even though a predominant direction was often observed in

each culture. We computed the speed of Up state propagation across the culture, relying on the onset time of individual neurons extracted through peeling algorithm, as described in the previous section. In detail, when a predominant direction is observed: we consider the onset time of the averaged trace t_0^A and collected the onset time t_0^n and the spatial coordinate $c^n = (x^n, y^n)$ of single neurons firing in a time windows $2\Delta t$ around t_0^A. We created a time bin vector t_0 that goes from $t_0^A - \Delta t$ to $t_0^A + \Delta t$ with an interval δt, which element t_0^i are:

$$t_0^i \in t_0, \qquad t_0^i = t_0^A - \Delta t + (i-1) * \delta t \qquad with \quad i \in \left[1, \frac{2\Delta t}{\delta t} + 1\right] \tag{2.2}$$

Time values t_0^n were approximated to the nearest t_0^i and sorted in descendent order. For each time bin value t_0^i, we calculated the relative centroid, or geometric center, of the activity $C(t_0^i) = C^i = (x^i, y^i)$, given by the arithmetic mean of the coordinates of the N_i neurons firing simultaneously in the instant t_0^i.

$$x^i = \sum_{m|t_0^m \to t_0^i} \frac{x^m}{N^i} \tag{2.3}$$

$$y^i = \sum_{m|t_0^m \to t_0^i} \frac{y^m}{N^i} \tag{2.4}$$

This points, that serve to identify "activity position" at each time step i, where linearly fitted to get the propagation direction $y = A * x + B$ and ortogonally projeced onto y, see Fig.2.7. We get the aligned points $C_p^i = (x_p^i, y_p^i)$, where:

$$x_p^i = A/(A^2 + 1) * (D^i - B) \tag{2.5}$$

$$y_p^i = A * x_p^i + D^i \tag{2.6}$$

where D^i is y-intercept of the line $y' = -1/A * x + D^i$ orthogonal to y and passing through (x^i, y^i).

$$D^i = y^i + 1/A * x^i; \tag{2.7}$$

We evaluate propagation speed as $V =< v_j >$:

$$v_j = \frac{\delta S^j}{\delta t} = \frac{\sqrt{(x^{j+1} - x^j)^2 + (y^{j+1} - y^j)^2}}{\delta t} \qquad with \quad j \in \left[1, \frac{2\Delta t}{\delta t}\right] \tag{2.8}$$

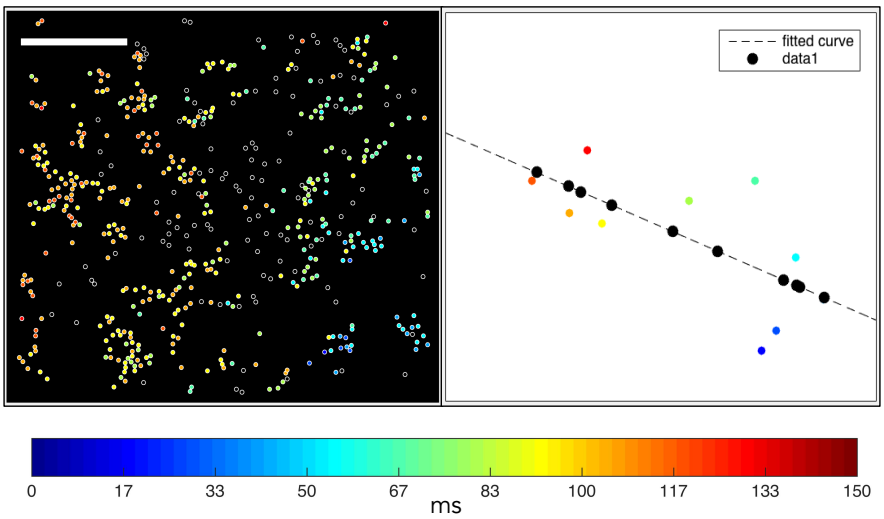

Figure 2.7: **Activity propagation.** Example of activity propagation along a particular direction. Events onset time of insividual neurons were used to determine the propagation direction and velocity. Scale bar: 500μm.

2.3.4 Network connectivity

Binary traces obtained from the analysis of fluorescence traces were processed to calculate the effective connections among neurons. In this thesis we used and compared two distinct methods: the transfer entropy function and the events coincidence function. Both methods enable to infer directed functional network connectivity in which the presence of a directed link between two nodes reflects the fact that knowledge of the activity of one node (source) is helpful in predicting the future behavior of another node (target). We consider that the synaptic time constants of the neuronal network ($\sim$ 1ms) are much

shorter than our time bin size (5ms/10ms). We therefore need to account for "same bin" causal interactions between nodes, i.e. between events that fall in the same time-bin. Additionally, as we discussed long, spontaneous network activity of sufficiently mature cultures switches between two dynamical regimes. Such cultures display period of sustained synchronous firing, Up states, combined with sparse irregular firing activity during Down states. Previous studies demonstrated that connectivity reconstruction depends on the dynamical state the network is in [48, 56]. Stetter et al. suggested that during the Up states, because of the high excitability and the collective synchronization of the network, there can happen that local events cause changes at very long distance which don't reflect a direct connection. Thus, during Up states the directed functional connectivity can diverge from the structural excitatory connectivity. On the contrary, in the relatively quiet Down period, a post-synaptic events is presumably influenced only by the pre-synaptic activity. To take it into account when reconstructing the network we have to restrict the evaluation of functional connectivity to non-synchronous dynamical state. We followed the method described in [48]: we selected dynamical states by introducing a variable, called Conditioning Level (*CL*), obtained from the histogram of the average signal of the whole network. We then include in the analysis all data points at time instants in which this average fluorescence is below *CL* value, located just on the right side of the Gaussian part of the histogram of the average fluorescence, see Fig.2.8**C**.

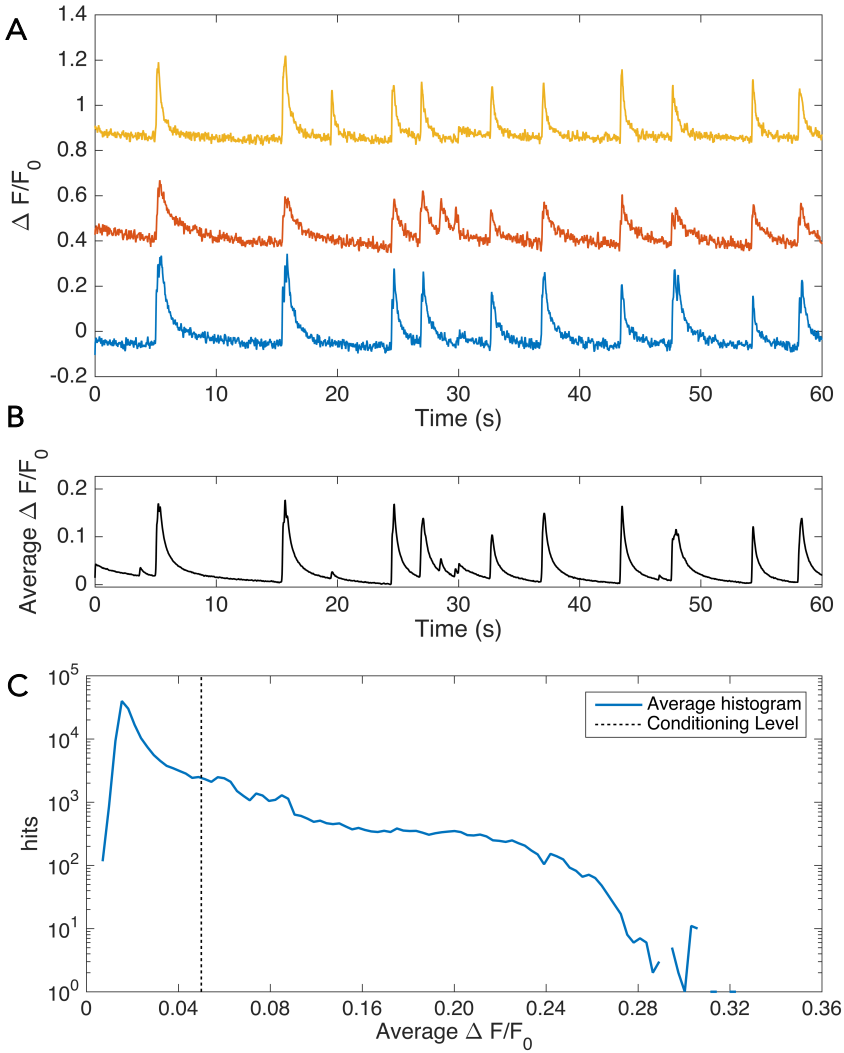

Figure 2.8: **Network activity and selection of dynamical states. A** Examples of calcium fluorescence time series for three neurons, vertically shifted for clarity. **B** Corresponding averages over the whole population of neurons. **C** Distribution of population-averaged fluorescence intensity for the complete time series, divided into two ranges. The functional connectivity associated to different dynamical regimes is then assessed by focusing the analysis on specific amplitude ranges.

Generalized Transfer Entropy

For two discrete Markov processes X and Y (here shown for equal Markov order k), the Transfer Entropy (TE) from Y to X was defined as:

$$TE_{Y\to X} = \sum P(x_{n+1}, x_n^{(k)}, y_n^{(k)}))log\frac{P(x_{n+1}|x_n^{(k)}, y_n^{(k)})}{P(x_{n+1}|x_n^{(k)})} \quad (2.9)$$

TE quantifies the flow of information directed from X to Y. It goes from 0 to infinity, where 0 indicates lack of causality from X to Y and a value ¿ 0 indicates the presence of causality. By definition, transfer entropy is directional and dynamic, being asymmetric and defined on transition probabilities. It can be seen as the distance in probability space (known as the Kullback-Leibler divergence [57]) between the "single node" transition matrix $P(x_{n+1}|x_n^{(k)})$ and the "two nodes" transition matrix $P(x_{n+1}|x_n^{(k)}, y_n^{(k)})$. To reconstruct functional connectivity from binary traces of network activity, we used and customized a previously described improved algorithmic approach based on a generalized version of TE, which take into account the general characteristics of the system [48]. This consists in modifying TE in two main aspects: the inclusion of "same bin" interaction and the selection of dynamical state. It is important to consider causal interactions between events that occur within the same time-bin because the precision with which events ignition is inferred (5 ms) is not high enough to extract the temporal order of elementary spiking events. Slower interactions are still included by calculating TE for a Markov order 1 and 2. In addition, the restriction of TE evaluation to non-synchronous dynamical states is crucial to properly capture interactions between neurons. Selection of dynamical states is performed by analyzing the histogram of the average signal of the network, and choosing a threshold value just on the right side of the Gaussian part, Fig.2.8.

Events Coincidence

We defined an alternative measure of effective functional correlation that we called Events Coincidence (EC). EC, whose algorithm

was developed in Pyton environment, for each event of each neuron, looks for the presence of an event of another neuron within a certain time interval Δt. Thus, for each pair of neurons X and Y, $EC_{X\to Y}$ represents the number of events coincidences revealed, normalized to the number of total spikes of the source neuron. By definition EC, detect the causal influence of events in the past with events at a later time, thus is asymmetric and directional. As for TE evaluation, EC takes into account "same bin" coincidences, and was calculated in time instants in which the network is in the non-synchronous dynamical regime.

Validation of connectivity index

Connectivity indices, calculated through generalized TE and EC functions, must be subjected to a selection process in order to eliminate non-significant connections, due to spurious and non-real correlations between neurons. Therefore it is necessary to establish a method to quantify index statistical significance. The easier way to determine whether the computed connectivity value is significant above the noise level is to choose a threshold that represents the minimum value that corresponds to a significant transfer of information. However, connectivity values depend on the amount of information present, so neurons with higher firing rates will naturally have higher values. A more appropriate approach would be to define a threshold for each couple of neurons. Prior literature has found the creation of surrogate data to be an effective way to determine whether the connectivity values are significant, using methods such as jittering [59, 60], shuffling of trials [61], and shuffling of inter-spike-intervals [62]. These methods estimate the distribution of a quantity by resampling original data. In this work we used a jittering algorithm, in which surrogate baseline data are generated from original data by moving each event time by a certain random offset. We constructed the offsets using a uniform random distribution from -6 time-bins to 6 time-bins (-30 to 30 ms). For each recording we build 50 surrogate dataset and calculated corresponding connectivity index. This values serve as a baseline for insignificant index, providing, for each pair of neuron, the distribution

of index value obtained by chance, thus 95% confidence interval. The connectivity matrix is then filtered eliminating all connections that do not have a value outside their own confidence interval.

In silico model

To asses the performance of our algorithm we test it on a series of calcium fluorescence traces generated by simulating dynamics of a network with known ground-truth topology. To model network structure and dynamics we adapt a previously described method [24] to fit our experimental observation.

Network construction. We used cells coordinates extracted from real experimental data to construct an *in silico* model of cortical neuronal networks. Pyramidal neurons were modelled as circular cell bodies (somas) with fixed diameter φ_s = 15μm. We simulated axons growth from each soma in a quasi-straight path, to mimic realistic condition. Axons length was given by a Rayleigh distribution

$$p(\ell) = \frac{\ell}{\sigma_\ell^2} exp\left(\frac{-\ell^2}{2\sigma_\ell^2}\right) \tag{2.10}$$

Where $\sigma_\ell^2 = 900\mu m$ to obtain $< \ell > \simeq 1.1mm$. We simulated fluctuation by dividing the total length ℓ into small segments ($\Delta\ell$), placing each segment at the end of the previous one and oriented according to a Gaussian distribution around the previous segment given by

$$p(\theta_i) = \frac{1}{\sqrt{2\pi\sigma_\theta^2}} exp\left(-\frac{(\theta_i - \theta_{i-1})^2}{2\sigma_\theta^2}\right) \tag{2.11}$$

where θ_{i-1} is the angle between the segment i-1 and the x-y plane. σ_θ is chosen to obtain a long persistence length ($\simeq 15^\circ$).

Finally, we modelled the dendritic tree of a neuron as a disk of diameter φ_s, following the work of Wen et al. [63]. The diameter was drawn from a Gaussian distribution with mean μ = 300μm and standard deviation of σ^2 = 40μm. The growth process described above leads to a geometric construction of the network connectivity based on the following rules: a connection can be established only when the axon of a given neuron intersects the dendritic tree of any other neuron,

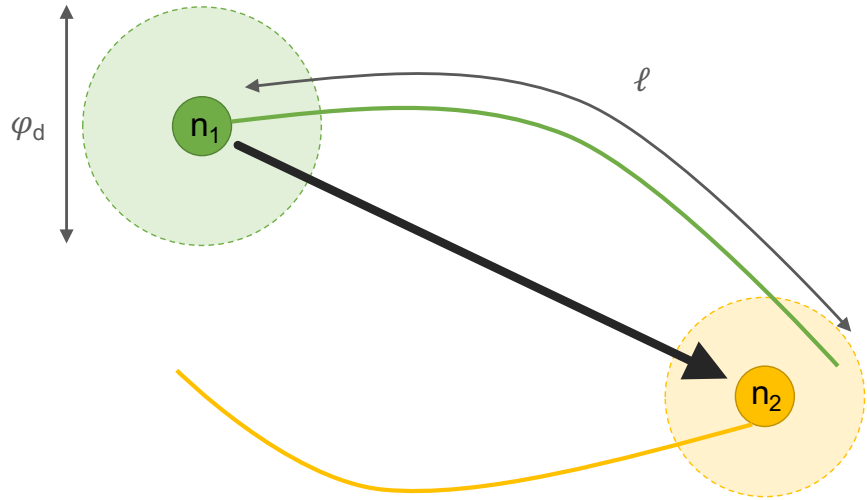

Figure 2.9: **Geometric construction of the neuronal network.** For simplicity only two neurons are shown,indicating their somas and axons. The area covered by the dendritic tree is depicted for two neurons. A connection between two neurons is established with a certain probability whenever the axon of a neuron crosses the dendritic tree of another one.

those neurons that fulfill this geometric condition will connect with probability α (in our case we considered α in the range 1/3–1). The whole network connectivity that results from this geometric construction is stored in the adjacency matrix A, where A$_i j$ = 1 identifies a connection i $\rightarrow$ j.

Soma dynamics. We simulated soma dynamics and action potentials generation using a a reduced form of a quadratic integrate-and-fire model with adaptation [64, 65].

$$\tau_c \frac{dv}{dt} = k(v - v_r)(v - v_t) - u + I + \eta, \tag{2.12}$$

$$\tau_\alpha \frac{du}{dt} = b(v - v_r) - u, \tag{2.13}$$

$$\text{if } v > v_p \text{ then } v \rightarrow v_c, u \rightarrow u + d$$

where $v(t)$ is the soma membrane potential, u accounts for the internal slow currents generated by the activation potassium channels and the

inactivation of sodium channels; I is the synaptic inputs from other neurons; and η is a noise term. The quadratic part $(v - v_r)(v - v_t)$ of equation 2.4 has two fixed points, one stable, v_r, and one unstable, v_t. These points characterize the dynamics of the neuron. Insufficient stimulation keeps $v < v_t$ and the membrane potential relaxes towards its resting potential v_r. However, repeated stimulation brings v above the threshold value v_t. The potential then grows rapidly up to a preset peak value $v \geq v_p$ that is associated to the generation of a spike. The potential is thereafter reset to v_c.

Synaptic dynamics. The total input currents on a neuron j is

$$I_j(t) = \sum \sum E_i(t, t_m) \tag{2.14}$$

where $E_i(t, t_m)$ is the current induced by neuron i at time t as a result of the action potential generated at time t_m. The first summation comprises all input connections k_{in}^j on neuron j, and the second one all spikes previously generated. The post-synaptic currents due to the firing of neuron i can be expressed as

$$E_i(t, t_m) = g_A D_i(t_m) exp\left(-\frac{t - t_m}{\tau_A}\right)\Theta(t - t_m) \tag{2.15}$$

where g_A is the strength of the synapse (associated to the receptor density at the post-synaptic terminal) and τ_A the characteristic decay time of the post-synaptic current. $D(t)$ accounts for short-term depression, a mechanism in which synapses reduce their efficacy due to depletion of neurotransmitters in their presynaptic vesicles [66].

Sources of noise. The last term of equation 2.4 accounts for the noise present in the system. We consider that two sources of noise: a Gaussian white noise associated to fluctuations in membrane potential and a shot noise representing the spontaneous release of neurotransmitters in the presynaptic terminals [24].

Chapter 3

A preliminary study: light effect on neuronal cultures

3.1 Introduction

In section 1.4, we have seen how optical techniques provided neuroscientists with a powerful new range of tools for controlling neuronal activity [14]. This techniques have the advantages of being contact-free, damage-free, artifact-free and spatially precise. However, light on its own is not completely inert. Several studies report that light at different wavelength and intensity, may alter cellular physiology [58]. Since 60's infrared light has been known to have effect on nerve cells [67, 68] and subsequently infrared neural stimulation (INS) was proposed as an alternative approach to achieve optical stimulation of neurons without the need for any genetic manipulation [69, 70]. INS consists in short pulses of infrared light directly absorbed by water [71, 72]. Nevertheless, infrared techniques require delivery of high power pulses and have to compete with strong absorption in water. In the past few years some investigations brought the attention to the effects of light in the visible spectrum on naive neurons. A recent work illustrates a significant inhibitory effect of blue and yellow LED light (470-570 nm range,13 mW) on the firing activity of different cell types (Mitral Cells and Tufted Neurons in the olfactory bulb and Medium Spiny Neurons in the striatum) [73]. Other previous studies

documented an excitatory effect of blue light on cortical neuron type [74, 75]. In all these works, the effect of light exposure appears to be due to an increase in bath or tissue temperature which leads to changes in resting membrane potential, spontaneous spiking, input resistance, membrane time constant, and synaptic activity in acute slices [76] [77] [78]. The present chapter will describe a preliminary work aimed to investigate and characterize the effects of visible LED light on naive primary cortical neurons activity. We demonstrate that a shift in light power (from $0.13mW/mm^2$ to $1.8mW/mm^2$) increases overall spontaneous calcium activity (29%). Earlier studies identified one of the potential mechanism behind optical stimulation of neurons in the activation of heat-sensitive ion channels TRPV [79, 80]. Different TRPV channels activate at different temperatures. The complete characterization of this effect is out of the scope of this work, nevertheless, we also investigated the role of the TRPV4 (sensitive to the temperature changes [51, 52, 53], and responsible for neural activation in the framework of the INS technique [79]) in the measured effect, which has been elsewhere addressed. We demonstrate that by blocking this channel, the activity enhancement effect disappears.

3.2 Experimental Methods

Primary neuronal cultures used in these experiments were prepared from the brain of 0-2-d-old C57BL/6 mice using culturing protocols described in section 2.1.2. Here we used 4-AP in order to increase calcium events frequency in culture with poor spontaneous activity. Both with and without 4-AP, the experiments were repeated after the addition of 5 μM concentration of RN1734, a blocker of TRPV4 channel. Additional experiments were done following the blockage of electrical activity through 1 μM TTX administration. See section 2.1.4 for more information about 4AP, RN1734 and TTX administration. Measurements of neuronal calcium activity were carried out at DIV 7-14 using custom-made fluorescence microscope described section 2.2.

Calcium imaging. Calcium imaging measurements were done under

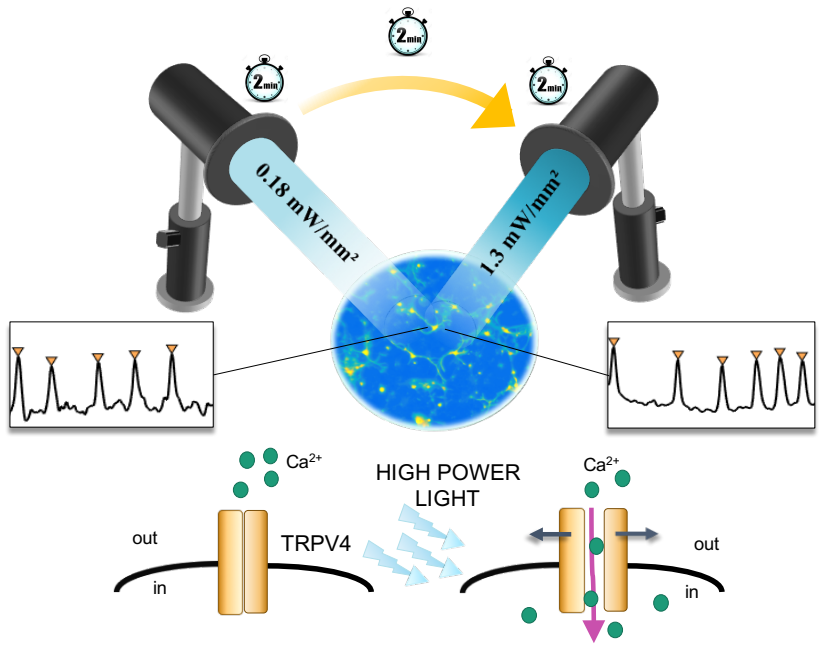

Figure 3.1: Experimental procedure. Two calcium imaging measurements were performed on the same area of the sample at low ($0.18mW/mm^2$) and high ($1.3mW/mm^2$) LED power illumination.

two experimental conditions (Fig.3.1b): in a first moment data were recorded using low-power light for excitation $0.18mW/mm^2$) and after 2 minutes a second measurement was performed on the same area of the sample using high-power illumination ($1.3mW/mm^2$). A third measurement at low-power light was done to check the reversibility of the phenomenon. Spontaneous activity was recorded as image sequences of 150-300 s in duration, with an acquisition speed of 1 Hz. Low acquisition speed was required to have enough signal-to-noise ratio in low-power measurements.

Patch Clamp. Additional electrophysiological recording were performed on Fluo-4 loaded neurons. Electrophysiological recording chamber was placed under an upright microscope (Olympus BX51WI) equipped with a 14 bit CCD camera system (Cool SNAP Myo, Photometrics). Fluorescence was achieved using a Cairn Research - Op-

toScan monochromator and visualized with a 40x water-immersion objective. The system was driven by Metafluor (Molecular Devices, Foster City, CA, USA). Membrane currents were recorded with the patch-clamp amplifier (Multiclamp 700B; Molecular Devices) and acquired with Clampex 10 software (Molecular Devices). Fluo-4 loaded neurons were placed in the recording chambers replacing culture medium with NES. Patch clamp recordings were obtained in whole-cell configuration, using borosilicate glass electrodes (4–5 M) filled with an intracellular solution containing (in mM): 140 KCl, 10 HEPES, 2 Mg-ATP, 0.01 $CaCl_2$, $2MgCl_2$, and 0.5 EGTA (pH =7.3 with KOH; osmolarity 290 mOsm). Neurons were voltage clamped at -70 mV for sEPSC recordings. Currents were filtered at 2 KHz, digitized (10 KHz) and acquired with Clampex 10 software (Molecular Devices).Neuronal activity was recorded in presence of fluorescent light ($1.4mW/mm^2$; wavelength 488; exposure 100-150 ms) for 10-12 minutes, after their sEPSCs (excitatory postsynaptic currents) were monitored for 5 minutes in absence of fluorescence. In control experiments, cells were recorded for 15 minutes in absence of fluorescent light.

3.3 Statistics

Calcium imaging. For each area and each value of the power intensity, data were acquired and saved as three-dimensional matrix, a sequence of 1600x1600 pixels images. Data analysis was performed as described in section 2.3 except for neurons identifications. Here centroids were extracted by analyzing the mean frame over time of the high power recording (instead of the cumulative difference of the signal between the various frames of the time series): we selected the most intense cells in order to reduce signal-to-noise ratio (SNR), especially in noisy low power measurements. Once the cells positions had been retrieved (500 - 800 for each area scanned), their fluorescence intensities traces as a function of time were collected, both in low and high power conditions. Calcium events detection was performed as previously illustrated, see sec.2.3. We recognized and discarded non-neuronal signals by analyzing calcium transients dynamics and

discarding calcium transients with a rise time higher than 2 seconds. In the total 4 minutes recording (2 min low power, 2 min high) from 60 to 150 spontaneously active neurons were found for each glass. To determine the effect of light power, the number of calcium events in low power condition and high power condition were statistically compared, through a paired unilateral Wilcoxon rank sum test. We obtained a certain number "*n*" of glass in which light power significantly increases the number of calcium events. To establish if these positive results are due exclusively to a repetition of type I error and thus the null hypothesis ('light power increase don't augment number of calcium events') is true, we calculated the probability to get by chance "*n*" statistically significant results over N total glass measured, as:

$$p = \sum_{m=n}^{N} \binom{m}{N} \alpha^m (1-\alpha)^{N-m} \tag{3.1}$$

Where α is the probability that the test failed rejecting the null hypothesis (0.05). The relative increase was calculated for each neuron and the average increase was calculated as:

$$\left\langle \frac{Events_H - Events_L}{Events_L} \right\rangle \tag{3.2}$$

We performed a populations analysis computing the mean number of events, the average events shape and network synchronization on each slide showing significat increment of neuron-by-neuron activity. We compared values obtained at low and high power by Wilcoxon rank sum tests. Synchronicity of the network was evaluated as the relative number of simultaneous neural events.

Patch Clamp. For patch clamp data analysis, sEPSCs were identified on the basis of a template created for each neuron using 30-50 single events for each trace. All events, recognized through the template search function, were visualized, identified and accepted by manual analysis. Data were analyzed off line with Clampfit 10 software; Origin 7 software was used for statistical analysis of electrophysiological recording.

3.4 Results

We exploited a wide field high-resolution calcium imaging setup to study the influence of LED illumination on spontaneous calcium activity of primary cortical neurons from early post-natal mice. By DIV 7 neuronal cortical cultures formed an active network and showed spontaneous activity. We recorded spontaneous calcium transients on 12 mm glasses at DIV 7-14, loading cells with Fluo-4 AM. For each slide we scanned several large areas (2x2 mm^2) and for each area we performed two measurements: one using low-power LED light (490 nm wavelength, 120 s, 0.18 mW/mm^2) for excitation, the other using higher LED power illumination (490 nm wavelength, 120 s, 1.3 mW/mm^2) Fig.3.1). Data from 2 minutes recording were collected and analyzed through a custom-made algorithm designed to recognize cells Fig.2.4, select neuronal traces and sort calcium events, discarding events characterized by slow rise time typical of astrocytes. We analyzed a total of 65 areas from N=12 slides from 5 different cultures. For each slide from 60 to 150 spontaneously active neurons were detected and the number of calcium events per neurons, at low and high power, were statistically compared (paired unilateral Wilcoxon rank sum test) to evaluate the effect of light power. On n=9 over N=12 (75%) slides scanned, light induced a significant (p¡0.05) enhancement of activity, namely an increase in number of calcium events per neurons as exemplified in Fig.3.2a-b. The validity of these results is assessed by the probability to obtain by chance "*n*" significant events over N experiments, i. e. the probability to repeat type I error n time, which is $p = 3.7 * 10^{-10}$. The average relative increase per neuron was 29 ± 6 %. The phenomenon was reversible, as the number of calcium events came back to control values on 75 % of slides when cultures were then exposed to the low power light stimulation ($p = 3.7 * 10^{-10}$) Fig.3.2g. Populations analysis were done by selecting statistically significant slides and comparing the average proprieties (number of events, amplitude and time constants) from low and high power measurements. We observed that relative high power illumination induces a significant increase in the mean number of events (p=0.002, N=9, rank sum test) without affecting the events

amplitude, rise and decay time constants ($p>0.05$, N=9, rank sum test) as shown in Fig.3.2c. Notably, the increase in network activity does not affects the network synchronization ($p>0.05$, N=9, rank sum test), measured as the relative number of simultaneous events (Fig.3.2c).
Parallel patch clamp recordings of spontaneous network activity on primary cortical neurons loaded with Fluo-4 AM confirmed that the switch-on of a fluorescent light source (488 nm, 1.4 mW/mm^2, fluorescent light exposure: 100-150 every second) significantly increases synaptic currents frequency by 86% (n = 6; *$p < 0.05$, paired t-test) Fig.3.2e, without affecting sEPSC amplitude (9.2 ± 2.8 pA control; 8.2 ± 1.2 pA, 488 nm light on; n = 5; $p > 0.1$, paired t-test; data not shown), suggesting an increase on neurotransmitters release. The increase in sEPSC frequency was not simply due to the switch-on of the 488 nm Fluorescence light; indeed, when the experiments were performed either on Fluo-4 AM loaded cells without light switch-on, or in unloaded cells exposed to the same light stimulation, the sEPSC frequency remained unaltered ($p > 0.4$, n = 6 paired t-test; Fig3.2f)).
To investigate the mechanisms involved in the light-induced effect observed, we repeated calcium imaging experimental protocol on cultures under different conditions: treated with 4-Aminopyridine (4-AP, 2 mM), a K^+ channel blocker; in the presence of tetrodotoxin (TTX,1μM), a selective blocker of voltage-activated sodium channels; in calcium free extra-cellular solution (0 calcium, 1 mM EGTA); in the presence of RN1734 ($5\mu M$), a selective antagonist of termosensitve TRPV4 in the co-presence of 4-AP and RN1734.
Cultures treated with 4-AP showed an enhanced spontaneous and synchronous activity compared to control, but the effect of light power on these cultures gave similar results: the increase in light power caused a significant increment of calcium events on 75% of the slides (ranksum $p = 4 * 10^{-7}$, N=8 slides , from 4 cultures, 42 total area, 1000 neurons) Fig.3.3b). The average increase per neurons was $58 \pm 3\%$, almost twice of the average increment in absence of 4-AP. Population analysis results are reported in Fig.3.3c (rank sum, N=6).
Administration of TTX allowed to detect spontaneous calcium oscillations in the absence of spike driven calcium entry. By inhibiting action potential network activation the application of high power light failed

to enhance network activity (5 slides , from 1 cultures, 40 neurons) Fig.3.2h.
To disclose the source of calcium rise involved in the observed phenomenon, additional time lapse recording were performed in neuronal cultures maintained in calcium free medium. As expected we recorded a very low calcium activity and the light induced effect was undetectable (6 slides , from 2 cultures; data not shown). These data suggested that the observed enhancement of calcium transient frequency required calcium entry from extracellular space, rather than calcium release from internal stores.
There are multiple mechanisms that may underlie the calcium influx from the extracellular space. Previous studies ascribed the effect of light exposure on neuronal activity to an increasing in bath temperature. The importance of temperature for neural physiology is known: changing bath temperatures leads to changes in the functional state of neurons [76], [77][78]. In particular it was previously shown that upon light stimulation of neuronal cultures thermosensitive TRPV channels are activated [79], inducing calcium entry.

These effects can be imputed to the sensitivity of these channel to temperature gradients across the cell membrane. Different TRPV channels indeed were described to be temperature sensitive channels over a wide range of temperature gradients. In particular, TRPV4 were shown to respond to small variations in the temperature range (25-40 °C) typical of our experiments (32 °C) [51], [52], [53]. To highlight the role of these channels in the observed phenomenon, calcium transients were recorded in the presence of RN1734 , a selective antagonist of TRPV4 [81]. Data reported in Fig.3.4a show that the high power induced effect was prevented in cultures treated with RN1734 (p=0.23, 6 slides, from 5 cultures, 21 total area, 40 neurons) and in cultures treated with both RN1734 and 4AP (p=0.23, 5 slides , from 3 cultures, 17 total area, 175 neurons). In addition, whole-cell patch clamp experiments confirmed that in the presence of RN1734 the increase in spontaneous network activity frequency was abolished (Fig.3.4b). This ensemble of results confirmed that the activation of TRPV4 channels was responsible for the enhancement of network activity induced by high power light stimulation. We also measured

the firing rate as a function of the temperature, without retrieving a significant activity enhancement, thus we can ascribe our effect to a more complex interplay between the channel and exposure to light. The complex pathway leading to the measured effect needs thus further investigation which is out of the scope of this work. Possible causes may be connected with the interaction with a different receptor, or to a possible sensitivity of the TRPV4 channels to temperature gradients between the internal (absorbing) volume of the cell and the (transparent), recording medium.

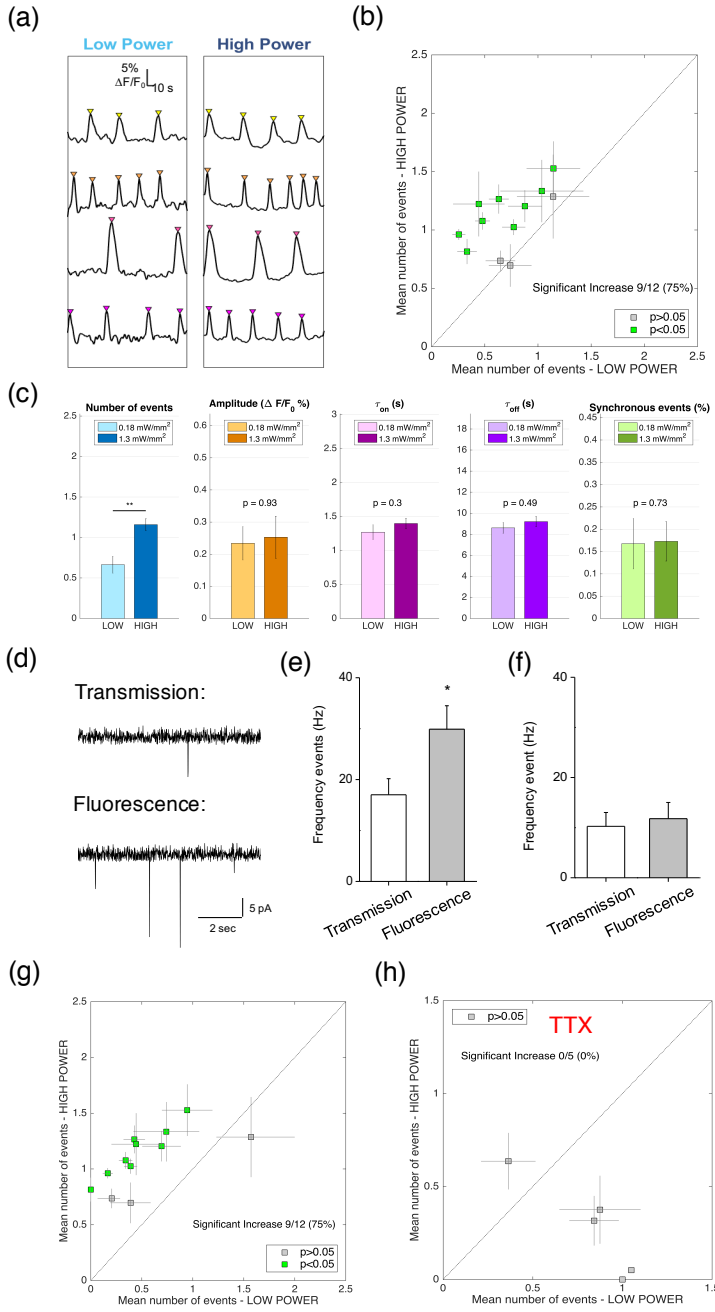

Figure 3.2: *Caption on next page...→*

Figure 3.2: ←...*figure on previous page.* (**a**) Representatives fluorescence intensities traces of four individual neurons from low (left) and high (right) light power measurements. (**b**) Effect produced by increasing LED power on 12 slides. (**c**) Populations analysis: mean number of events, peaks amplitude, rise time constant, decay time constant and synchronization, in low and high power conditions. Rank sum test, N=9. (**d**) Representative traces of spontaneous neuronal activity of whole-cell recordings from Fluo-4 loaded primary cortical neurons, under transmission illumination (upper trace) and under exposure to fluorescence illumination (488 nm, 1.4 mW/mm^2; lower trace). (**e**) Bar graph of corresponding mean frequency event measured before (white bar) and after (gray bar) exposure of cells to fluorescence illumination. (**f**) Mean frequency event measured in unloaded primary cortical culture by patch clamp recordings, before (white bar) and after (gray bar) exposure of cells to fluorescence illumination. (**g**) Number of calcium events came back to control values when cultures are exposed again to low power light after high power stimulation. (**h**) Results obtained by increasing LED power on 5 slides treated with TTX.

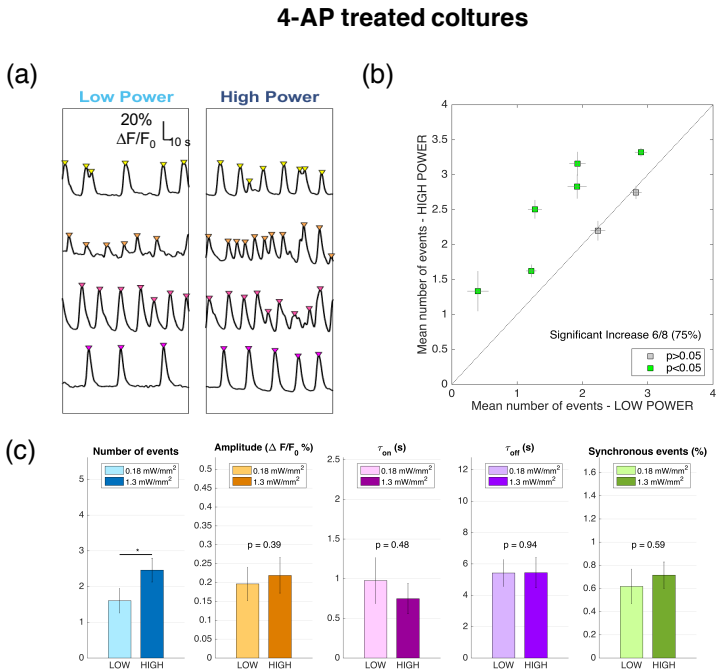

Figure 3.3: (**a**) Representatives fluorescence intensities traces of individual neuron filtered with a modified Perona-Malik filter from low (left) and high (right) light power measurements in cultures treated with 4-AP. (**b**) Effect produced by increasing LED power on 8 slides treated with 4-AP $p = 4 * 10^{-7}$. (**c**) Populations analysis in cultures treated with 4-AP: mean number of events, peaks amplitude, rise time constant, decay time constant and synchronization, in low a high power conditions. Rank sum test, N=6.

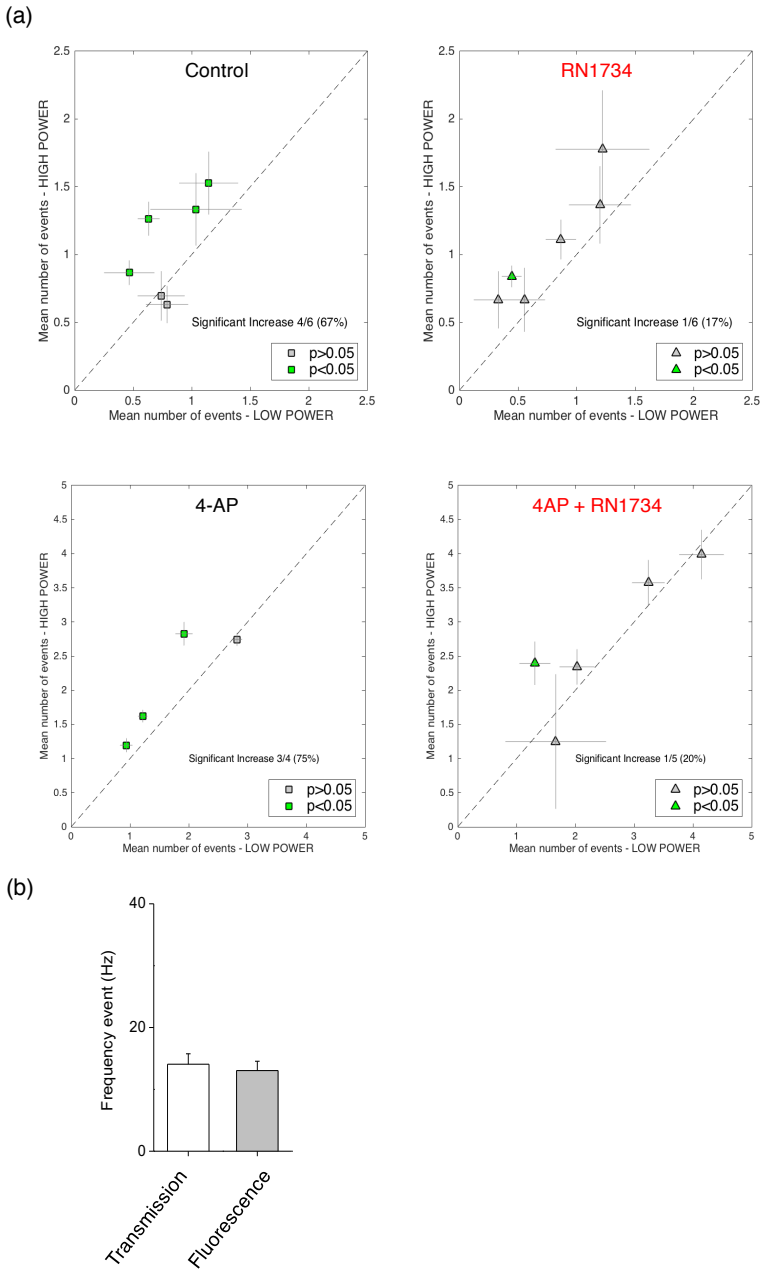

Figure 3.4: (**a**) Effect produced by increasing LED power in various condition: control (top-left), with 4-AP (bottom-left), with RN1734 (top-right) and with both 4-AP and RN1734 (bottom-right). *Continue on next page...*→

Figure 3.4: ←*...begin on previous page.* Data from control measurements (Rank sum test, $p = 8.6 * 10^{-5}$, $p = 4.8 * 10^{-4}$) were compared with data recorded under blockage of TRPV4 channels (Rank sum test, p=0.23). (**b**) Mean frequency event measured in Fluo-4 loaded primary cortical culture treated with RN1734 (5 mM, TRPV4 blocker). Patch clamp recordings showed that in presence of the TRPV4 blocker, inter-event interval of spontaneous synaptic events was not increased by the exposure to the fluorescent light (transmission: 77.9 $\pm$ 11.9 ms; fluorescence light: 82.7 $\pm$ 10.6 ms; n = 6; p $>$ 0.4, paired t-test).

3.5 Discussion

Our results are in accordance with previous studies reporting an excitatory effect of visible light exposure on cortical neurons *in vivo*. Christie et al. (2013) recorded an fMRI signal in a rat cortex while exposed to blue laser light stimulation and Stujenske, Spellman, & Gordon (2015) observed an increasing of prefrontal cortex firing activity in living mice upon laser stimulation at 532 nm. Both studies attributed the activity enhancement to a rising in tissue temperature. It was previously shown that neurons express transient receptor potential channels (TRPV) acting as sensory mediators and activated by endogenous ligands, temperature, mechanical and osmotic stress [51]. The components of this channels family contribute to the increase of intracellular calcium by providing or modulating Ca^{2+} entry pathways, and by releasing Ca^{2+} from intracellular stores [82].
In summary, we investigated the effect of the illumination power on neuronal network activity on *in vitro* cortical cultures, using a custom-made optical setup. We describe a light-induced increase of synaptic activity mediated by the activation of TRPV4. We demonstrated by optical and patch clamp experiments that high power LED exposure transiently increased calcium events and spontaneous network activity on cortical cultures, without affecting transients shape (amplitude, rise and decay time) and network synchronization. Moreover, patch clamp experiments made on neurons stimulated by high power light, in the absence of Fluo4-AM loading, demonstrated that the fluorophore and light together are necessary to increase sEPSC frequency. Thus these data suggested that, during LED exposure, the Fluo-4 light absorption caused a release of thermal energy inside the cell and the activation of the thermosensitive channels TRPV4. These results warn who performs calcium imaging and optogenetics experiments about possible undesired effect on neuronal activity, which should be taken into account. Moreover, even if further studies are necessary to better understand the mechanism behind this phenomenon, our results pave the way to the exploitation of optical stimulation to non-invasively modulate brain signaling avoiding genetic manipulation.

Chapter 4

Results

In this chapter we will show results obtained by analyzing recordings of spontaneous network activity in sample model of Alzheimer's Disease. We collected data from primary cortical cultures derived both from 3xTg and B6/129 mouse strains, Alzheimer's model (AD) and Wild Type (WT), respectively. Measurements of neuronal calcium signals were carried out at 6-30 days in vitro (DIV), on different sized cultures (see sec.2.1.3), using the custom-made fluorescence microscope described in section 2.2. We recorded 10 minutes of activity with acquisition frequency set to 50 Hz and 2x2 mm^2 field of view. To evaluate the influence of inhibitory control on the emergent activity of the cortical network, some experiments were repeated after the blockage of inhibition (through the addition of 5 μM Bicucculine, see sec.2.1.4).

4.1 Cortical Slow Oscillation

We recorded spontaneous cortical oscillatory activity (SO), which is characterized by alternating periods of intense neuronal firing (Up states) and rather quiescent periods regimes (Down states), in different conditions. Several parameters of the SO were quantified and compared between 3xTg-AD and control cultures: the length of the Up state, the length of the Down state, the length of the whole Up-Down state cycle, their respective coefficients of variation (CV) and the

relative single neuron firing frequency during Up and Down states.

State duration in AD model vs Wild Type cultures

For each recording, the averaged fluorescence signal was used as indicator of the network collective dynamics to identify Up and Down states and evaluate their length, as explained in sec.2.3.2. First of all, we assessed how the duration of the different regimes is affected by the age of the culture both in AD and WT samples, fig. 4.1. While both WT and AD cultures show a similar significant decrease of the Down state and the whole cycle duration from early to mature stage, WT cultures also display a significant increased duration of the Up states with increasing age, while Up length in AD samples remained rather unaltered (with a slight tendency to increase). We assembled data in three group: from 6 to 13 DIV, from 13 to 19 DIV, more then 20 DIV. Mean Up state duration is lower in AD cultures since early mature stage and significantly differ from control at mature stages (ranksum test, DIV 14-19 p=,DIV$>$20 p=). The tendency of AD sample to have shorter Up states is not accompanied by significant alteration in the SO frequency or Down state length. Mean duration of whole cycle and Down states did not significantly differ between the 2 groups at any stage of maturation. Coefficients of variations remain stable at different stages, both in AD and WT and no significant differences were detected between two group. High CV values reflect high irregularity in both type of cultures at each maturation stage.

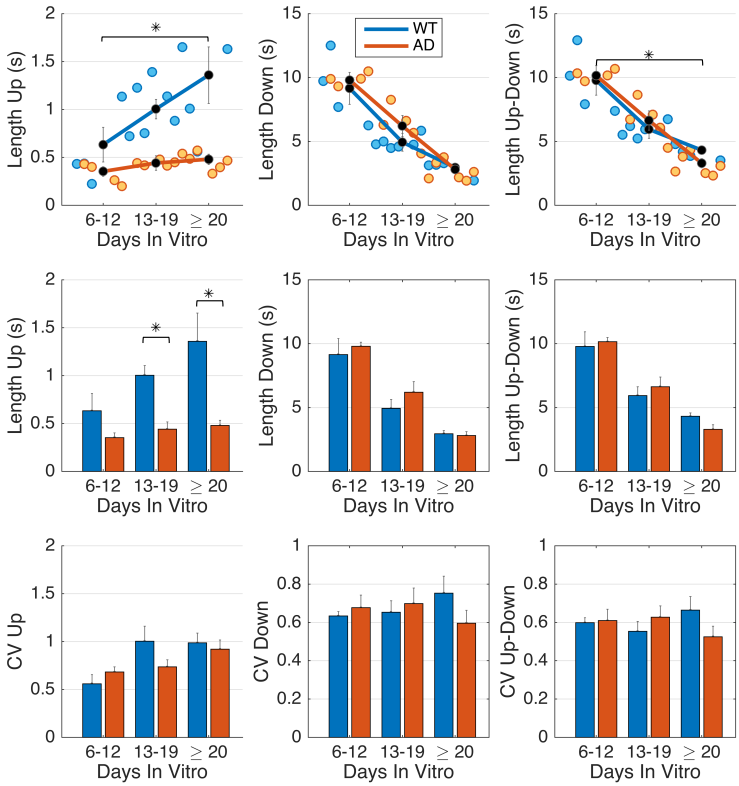

Figure 4.1: **SO property in AD model vs Wild Type cultures**

We also computed a measure of the firing rate of single neurons during Up states with respect to the activity during the Down states. Indeed, while it is true Down states are considered relatively silent states with respect to Up states, there is some firing in Down states. Fig. show that relative firing frequency during Up and Down states remain unaltered in AD sample respect to control.

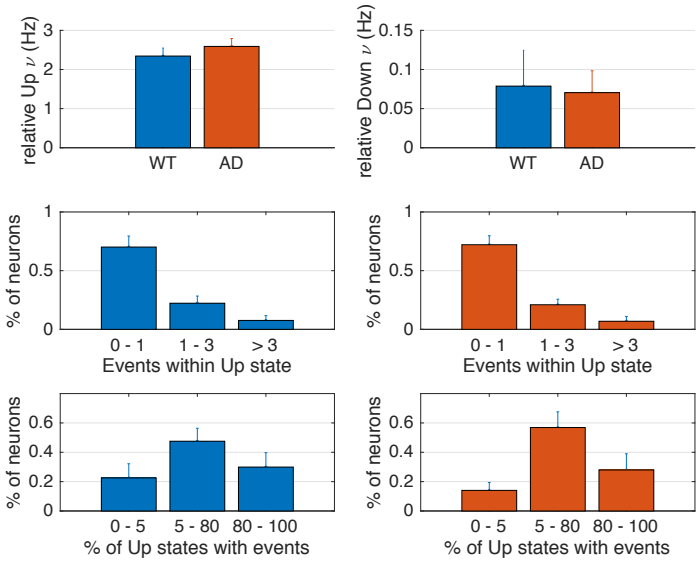

Figure 4.2: **Single neurons contribution.**

Inhibitory modulation of SO in AD model vs Wild Type cultures

It is agreed that excitation and inhibition balance each other both during spontaneous and during sensory activated cortical activity. We studied the functional contribution of inhibition to the slow oscillatory patterns generated by the cortical network, both in AD and control cultures. We measured activity in standard condition (excitatory + inhibitory network, E + I) and with blocked inhibition (only excitatory network, E). As aspected, the removal of inhibition induced a shortening of the Up states both in control and AD. The duration of the subsequent Down states was also modified, becoming longer and the same for whole cycle duration in both conditions. To quantify the effect due to inhibition blockage we evaluated the mean ratio of the states duration in E and E + I conditions. There were no statistically significant differences between AD and control.

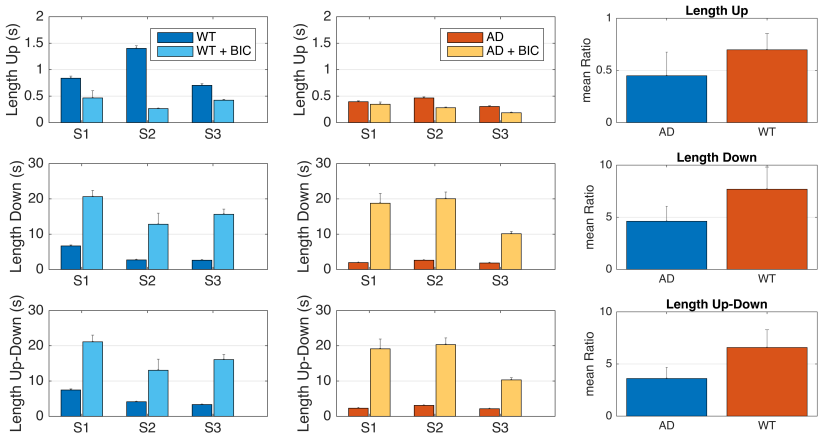

Figure 4.3: **Inhibitory modulation of SO**.

Scale free properties of SO

To evaluate the effect of culture size on spontaneous SO activity we compared periods length in small circular cultures with a diameter ϕ that range from 1.5 to 6 mm. No significant differences where observed among the different sized cultures. Shorter Up states in AD samples, respect to control were observed for each size, even if for smallest cultures ($\phi < 4$mm) it is not significant.

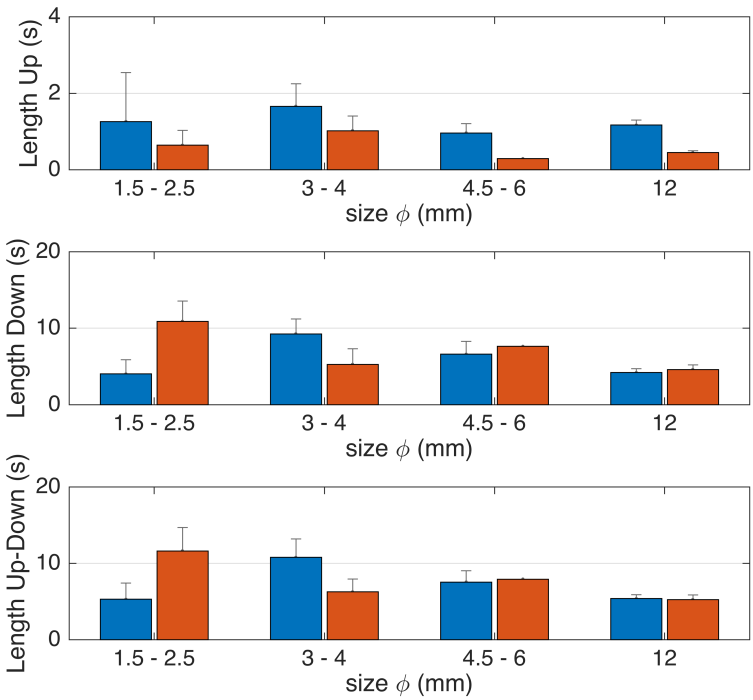

Figure 4.4: **SO properties in different sized cultures**

4.2 Signal propagation

4.3 Networks property

We used a generalization of Transfer Entropy method to inferring connectivity in neuronal networks based on fluorescence calcium imaging data. As described in sec.2.3, we extracted single neurons onset time with sub-sampling temporal resolution through an implemented peel algorithm, from each recording. Binary traced were used for TE calculation, implemented with two features, namely the inclusion of same bin interactions and the separation of dynamical states through conditioning of the fluorescence signal (see methods, sec.**??**). Once TE was calculated, it should be filtered to eliminate

non-significant connections. The easier way to determine whether the computed connectivity value is significant above the noise level is to choose a threshold that represents the minimum value that corresponds to a significant transfer of information. However, connectivity values depend on the amount of information present, so neurons with higher firing rates will naturally have higher values. For this reason it is more correct to establish a threshold proper for each neurons pair. In this work we used a jittering algorithm, in which we generated 50 surrogates baseline data from original data by moving each event time by a certain random offset, and calculated TE for each surrogates. The connectivity matrix is then filtered eliminating all connections that do not have a value outside their own confidence interval. On filtered adjacency matrix we evaluated network properties: nodes degree, clustering coefficient, path length and efficiency.

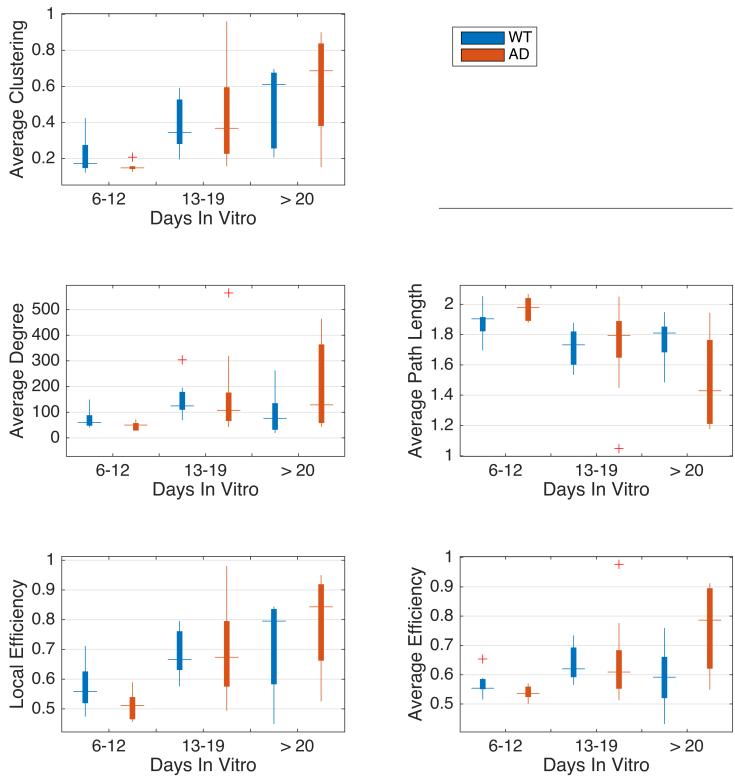

Figure 4.5: **Network properties at different stages.**

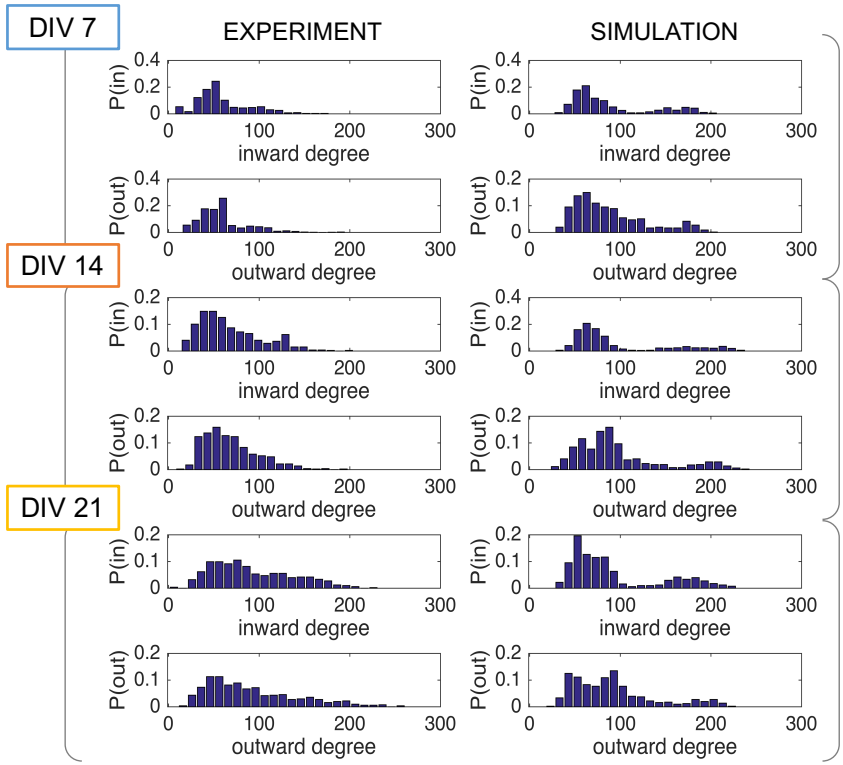

Figure 4.6: **Degree distribution.**

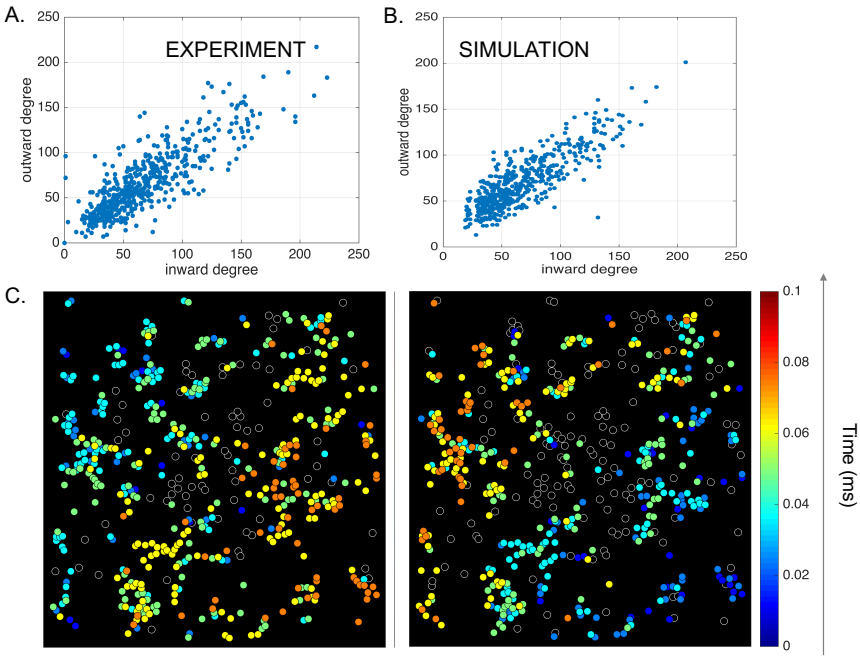

Figure 4.7: **Directionality.**

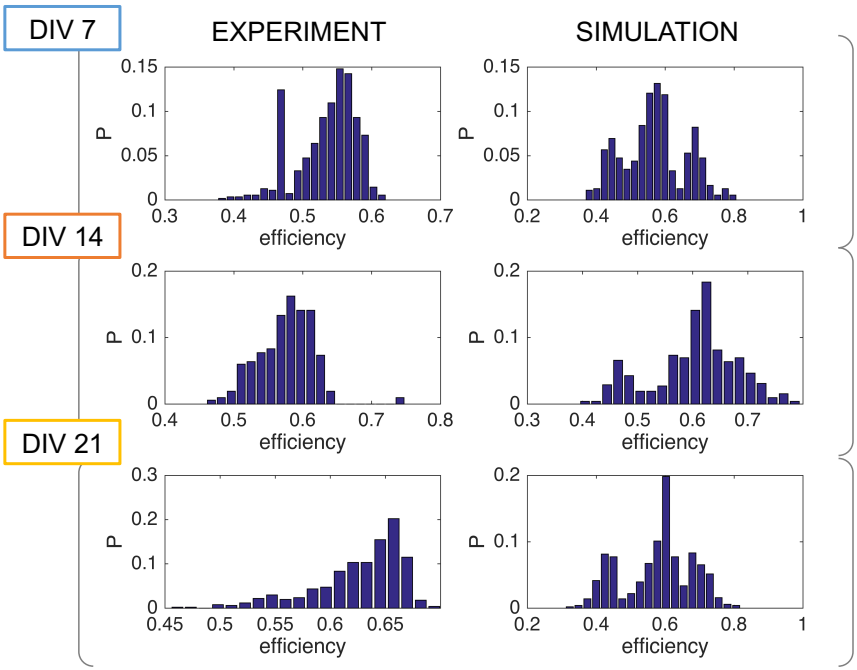

Figure 4.8: **Efficiency distribution.**

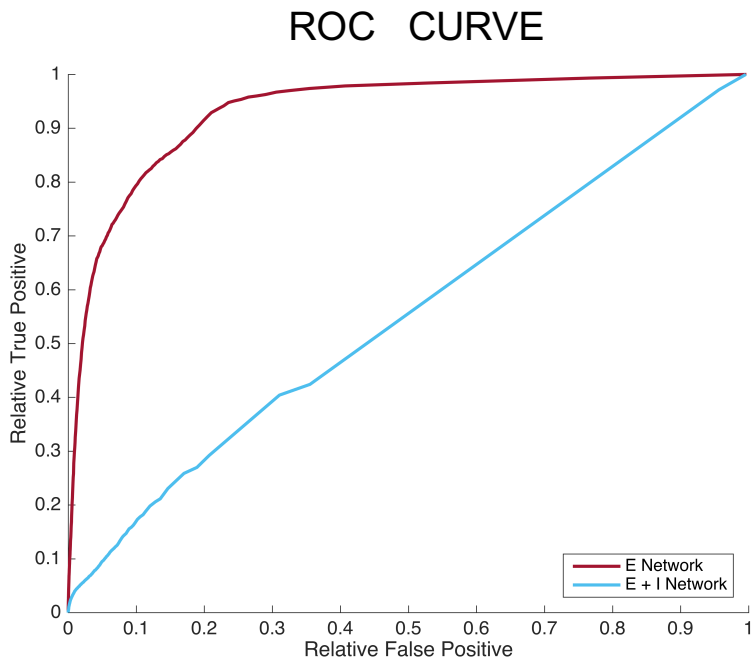

Figure 4.9: **ROC curves.**

Bibliography

[1] Ma'ayan, A. (2017). Complex systems biology. Journal of the Royal Society Interface, 14(134), 20170391.

[2] Rubinov, M., & Sporns, O. (2010). Complex network measures of brain connectivity: uses and interpretations. Neuroimage, 52(3), 1059-1069.

[3] Sporns, O., Chialvo, D. R., Kaiser, M., & Hilgetag, C. C. (2004). Organization, development and function of complex brain networks. Trends in cognitive sciences, 8(9), 418-425.

[4] Bollobás, B., & Béla, B. (2001). Random graphs (No. 73). Cambridge university press.

[5] Barabási, A. L., & Bonabeau, E. (2003). Scale-free networks. Scientific american, 288(5), 60-69.

[6] Dehaene, S., Cohen, L., Sigman, M., & Vinckier, F. (2005). The neural code for written words: a proposal. Trends in cognitive sciences, 9(7), 335-341.

[7] Rossi, U. (2003). The history of electrical stimulation of the nervous system for the control of pain. Pain research and clinical management, 15, 5-16.

[8] Sironi, V. A. (2011). Origin and evolution of deep brain stimulation. Frontiers in integrative neuroscience, 5, 42.

[9] Neher, E. (1992). [6] Correction for liquid junction potentials in patch clamp experiments. In Methods in enzymology (Vol. 207, pp. 123-131). Academic Press.

[10] Improved patch-clamp techniques for high-resolution current recording from cells and cell-free membrane patches

[11] Kanwisher, N. (2010). Functional specificity in the human brain: a window into the functional architecture of the mind. Proceedings of the National Academy of Sciences, 107(25), 11163-11170.

[12] Spira, M. E., & Hai, A. (2013). Multi-electrode array technologies for neuroscience and cardiology. Nature nanotechnology, 8(2), 83.

[13] Berdondini, L., Imfeld, K., Maccione, A., Tedesco, M., Neukom, S., Koudelka-Hep, M., & Martinoia, S. (2009). Active pixel sensor array for high spatio-temporal resolution electrophysiological recordings from single cell to large scale neuronal networks. Lab on a Chip, 9(18), 2644-2651.

[14] C Thompson, A., R Stoddart, P., & Jansen, E. D. (2014). Optical stimulation of neurons. Current molecular imaging, 3(2), 162-177.

[15] Zemelman, B. V., Lee, G. A., Ng, M., & Miesenböck, G. (2002). Selective photostimulation of genetically chARGed neurons. Neuron, 33(1), 15-22.

[16] Zemelman, B. V., Nesnas, N., Lee, G. A., & Miesenböck, G. (2003). Photochemical gating of heterologous ion channels: remote control over genetically designated populations of neurons. Proceedings of the National Academy of Sciences, 100(3), 1352-1357.

[17] Yang, W., & Yuste, R. (2017). In vivo imaging of neural activity. Nature methods, 14(4), 349.

[18] Pnevmatikakis, E. A., Soudry, D., Gao, Y., Machado, T. A., Merel, J., Pfau, D., ... & Ahrens, M. (2016). Simultaneous denoising, deconvolution, and demixing of calcium imaging data. Neuron, 89(2), 285-299.

[19] Mukamel, E. A., Nimmerjahn, A., & Schnitzer, M. J. (2009). Automated analysis of cellular signals from large-scale calcium imaging data. Neuron, 63(6), 747-760.

[20] Gladkov, A., Grinchuk, O., Pigareva, Y., Mukhina, I., Kazantsev, V., & Pimashkin, A. (2018). Theta rhythm-like bidirectional cycling dynamics of living neuronal networks in vitro. PloS one, 13(2), e0192468.

[21] Levina, A., Herrmann, J. M., & Geisel, T. (2007). Dynamical synapses causing self-organized criticality in neural networks. Nature physics, 3(12), 857.

[22] Downes, J. H., Hammond, M. W., Xydas, D., Spencer, M. C., Becerra, V. M., Warwick, K., ... & Nasuto, S. J. (2012). Emergence of a small-world functional network in cultured neurons. PLoS computational biology, 8(5), e1002522.

[23] de Santos-Sierra, D., Sendiña-Nadal, I., Leyva, I., Almendral, J. A., Anava, S., Ayali, A., ... & Boccaletti, S. (2014). Emergence of small-world anatomical networks in self-organizing clustered neuronal cultures. PloS one, 9(1), e85828.

[24] Orlandi, J. G., Soriano, J., Alvarez-Lacalle, E., Teller, S., & Casademunt, J. (2013). Noise focusing and the emergence of coherent activity in neuronal cultures. Nature Physics, 9(9), 582.

[25] Sanchez-Vives, M. V., & McCormick, D. A. (2000). Cellular and network mechanisms of rhythmic recurrent activity in neocortex. Nature neuroscience, 3(10), 1027.

[26] Sanchez-Vives, M. V., Massimini, M., & Mattia, M. (2017). Shaping the default activity pattern of the cortical network. Neuron, 94(5), 993-1001.

[27] Neske, G. T. (2016). The slow oscillation in cortical and thalamic networks: mechanisms and functions. Frontiers in neural circuits, 9, 88.

[28] Braitenberg, V., & Schüz, A. (1998). Cortical architectonics. In Cortex: Statistics and geometry of neuronal connectivity (pp. 135-137). Springer, Berlin, Heidelberg.

[29] Binzegger, T., Douglas, R. J., & Martin, K. A. (2004). A quantitative map of the circuit of cat primary visual cortex. Journal of Neuroscience, 24(39), 8441-8453.

[30] Douglas, R. J., & Martin, K. A. (2004). Neuronal circuits of the neocortex. Annu. Rev. Neurosci., 27, 419-451.

[31] Ruiz-Mejias, M., Ciria-Suarez, L., Mattia, M., & Sanchez-Vives, M. V. (2011). Slow and fast rhythms generated in the cerebral cortex of the anesthetized mouse. Journal of neurophysiology, 106(6), 2910-2921.

[32] Andersen, P., & Andersson, S. A. (1968). Physiological basis of the alpha rhythm (Vol. 1). Plenum Publishing Corporation.

[33] Steriade, M., Nunez, A., & Amzica, F. (1993). A novel slow (¡ 1 Hz) oscillation of neocortical neurons in vivo: depolarizing and hyperpolarizing components. Journal of neuroscience, 13(8), 3252-3265.

[34] Sanchez-Vives, M. V., Mattia, M., Compte, A., Perez-Zabalza, M., Winograd, M., Descalzo, V. F., & Reig, R. (2010). Inhibitory modulation of cortical up states. Journal of neurophysiology, 104(3), 1314-1324.

[35] Reig, R., Mattia, M., Compte, A., Belmonte, C., & Sánchez-Vives, M. V. (2009). Temperature modulation of slow and fast cortical rhythms. Journal of neurophysiology, 103(3), 1253-1261.

[36] Sancristóbal, B., Rebollo, B., Boada, P., Sanchez-Vives, M. V., & Garcia-Ojalvo, J. (2016). Collective stochastic coherence in recurrent neuronal networks. Nature Physics, 12(9), 881.

[37] Castano-Prat, P., Perez-Mendez, L., Perez-Zabalza, M., Sanfeliu, C., Giménez-Llort, L., & Sanchez-Vives, M. V. (2019). Altered slow (¡ 1 Hz) and fast (beta and gamma) neocortical oscillations in the 3xTg-AD mouse model of Alzheimer's disease under anesthesia. Neurobiology of aging, 79, 142-151.

[38] Castano-Prat, P., Perez-Zabalza, M., Perez-Mendez, L., Escorihuela, R. M., & Sanchez-Vives, M. V. (2017). Slow and fast neocortical oscillations in the senescence-accelerated mouse model SAMP8. Frontiers in aging neuroscience, 9, 141.

[39] Frazzini, V., Guarnieri, S., Bomba, M., Navarra, R., Morabito, C., Mariggiò, M. A., & Sensi, S. L. (2016). Altered Kv2. 1 functioning promotes increased excitability in hippocampal neurons of an Alzheimer's disease mouse model. Cell death & disease, 7(2), e2100.

[40] Hu, W. Y., He, Z. Y., Yang, L. J., Zhang, M., Xing, D., & Xiao, Z. C. (2015). The Ca 2+ channel inhibitor 2-APB reverses β -amyloid-induced LTP deficit in hippocampus by blocking BAX and caspase-3 hyperactivation. British journal of pharmacology, 172(9), 2273-2285.

[41] Stam, C. J., Jones, B. F., Nolte, G., Breakspear, M., & Scheltens, P. (2006). Small-world networks and functional connectivity in Alzheimer's disease. Cerebral cortex, 17(1), 92-99.

[42] Palop, J. J., & Mucke, L. (2010). Amyloid-β–induced neuronal dysfunction in Alzheimer's disease: from synapses toward neural networks. Nature neuroscience, 13(7), 812.

[43] Gimenez-Llort, L., Blazquez, G., Canete, T., Johansson, B., Oddo, S., Tobena, A., ... & Fernandez-Teruel, A. (2007). Modeling behavioral and neuronal symptoms of Alzheimer's disease in

mice: a role for intraneuronal amyloid. Neuroscience & Biobehavioral Reviews, 31(1), 125-147.

[44] Chen, Y., Liang, Z., Blanchard, J., Dai, C. L., Sun, S., Lee, M. H., ... & Gong, C. X. (2013). A non-transgenic mouse model (icv-STZ mouse) of Alzheimer's disease: similarities to and differences from the transgenic model (3xTg-AD mouse). Molecular neurobiology, 47(2), 711-725.

[45] Vale, C., Alonso, E., Rubiolo, J. A., Vieytes, M. R., LaFerla, F. M., Giménez-Llort, L., & Botana, L. M. (2010). Profile for amyloid-β and tau expression in primary cortical cultures from 3xTg-AD mice. Cellular and molecular neurobiology, 30(4), 577-590.

[46] Garofalo M, Nieus T, Massobrio P, Martinoia S (2009) Evaluation of the performance of information theory-based methods and cross-correlation to estimate the functional connectivity in cortical networks. PLoS One 4: e6482.

[47] Ito, S., Hansen, M. E., Heiland, R., Lumsdaine, A., Litke, A. M., & Beggs, J. M. (2011). Extending transfer entropy improves identification of effective connectivity in a spiking cortical network model. PloS one, 6(11), e27431.

[48] Stetter, O., Battaglia, D., Soriano, J., & Geisel, T. (2012). Model-free reconstruction of excitatory neuronal connectivity from calcium imaging signals. PLoS computational biology, 8(8), e1002653.

[49] Beaudoin III, G. M., Lee, S. H., Singh, D., Yuan, Y., Ng, Y. G., Reichardt, L. F., & Arikkath, J. (2012). Culturing pyramidal neurons from the early postnatal mouse hippocampus and cortex. Nature protocols, 7(9), 1741.

[50] Bostock, H., Sears, T. A., & Sherratt, R. M. (1981). The effects of 4-aminopyridine and tetraethylammonium ions on normal and demyelinated mammalian nerve fibres. The Journal of Physiology, 313(1), 301-315.

[51] Güler, A. D., Lee, H., Iida, T., Shimizu, I., Tominaga, M., & Caterina, M. (2002). Heat-evoked activation of the ion channel, TRPV4. Journal of Neuroscience, 22(15), 6408-6414.

[52] Watanabe, H., Vriens, J., Suh, S. H., Benham, C. D., Droogmans, G., & Nilius, B. (2002). Heat-evoked activation of TRPV4 channels in a HEK293 cell expression system and in native mouse aorta endothelial cells. Journal of Biological Chemistry, 277(49), 47044-47051.

[53] Nilius, B., Vriens, J., Prenen, J., Droogmans, G., & Voets, T. (2004). TRPV4 calcium entry channel: a paradigm for gating diversity. American Journal of Physiology-Cell Physiology, 286(2), C195-C205.

[54] Palazzolo, G., Moroni, M., Soloperto, A., Aletti, G., Naldi, G., Vassalli, M., ... & Difato, F. (2017). Fast wide-volume functional imaging of engineered in vitro brain tissues. Scientific reports, 7(1), 8499.

[55] Grewe, B. F., Langer, D., Kasper, H., Kampa, B. M., & Helmchen, F. (2010). High-speed in vivo calcium imaging reveals neuronal network activity with near-millisecond precision. Nature methods, 7(5), 399.

[56] Battaglia, D., Witt, A., Wolf, F., & Geisel, T. (2012). Dynamic effective connectivity of inter-areal brain circuits. PLoS computational biology, 8(3), e1002438.

[57] MacKay, D. J., & Mac Kay, D. J. (2003). Information theory, inference and learning algorithms. Cambridge university press.

[58] Deng, W., Goldys, E. M., Farnham, M. M., & Pilowsky, P. M. (2014). Optogenetics, the intersection between physics and neuroscience: light stimulation of neurons in physiological conditions. American Journal of Physiology-Regulatory, Integrative and Comparative Physiology, 307(11), R1292-R1302.

[59] Nigam, S., Shimono, M., Ito, S., Yeh, F. C., Timme, N., Myroshnychenko, M., ... & Masmanidis, S. C. (2016). Rich-club organization in effective connectivity among cortical neurons. Journal of Neuroscience, 36(3), 670-684.

[60] Walker, B. L., & Newhall, K. A. (2018). Inferring information flow in spike-train data sets using a trial-shuffle method. PloS one, 13(11), e0206977.

[61] Vicente, R., Wibral, M., Lindner, M., & Pipa, G. (2011). Transfer entropy—a model-free measure of effective connectivity for the neurosciences. Journal of computational neuroscience, 30(1), 45-67.

[62] Rivlin-Etzion, M., Ritov, Y. A., Heimer, G., Bergman, H., & Bar-Gad, I. (2006). Local shuffling of spike trains boosts the accuracy of spike train spectral analysis. Journal of neurophysiology, 95(5), 3245-3256.

[63] Wen, Q., Stepanyants, A., Elston, G. N., Grosberg, A. Y., & Chklovskii, D. B. (2009). Maximization of the connectivity repertoire as a statistical principle governing the shapes of dendritic arbors. Proceedings of the National Academy of Sciences, 106(30), 12536-12541.

[64] Izhikevich, E. M. Simple model of spiking neurons. IEEE Trans. Neural Netw. (1990-2011) 14(6), 1569–1572 (2003)

[65] Alvarez-Lacalle, E., & Moses, E. (2009). Slow and fast pulses in 1-D cultures of excitatory neurons. Journal of computational neuroscience, 26(3), 475-493.

[66] Golomb, D., & Amitai, Y. (1997). Propagating neuronal discharges in neocortical slices: computational and experimental study. Journal of neurophysiology, 78(3), 1199-1211.

[67] Arvanitaki, A., & Chalazonitis, N. (1961). Excitatory and inhibitory processes initiated by light and infra-red radiations in single identifiable nerve cells (giant ganglion cells of Aplysia) (pp. 194-231). New York: Pergamon Press.

[68] Fork, R. L. (1971). Laser stimulation of nerve cells in Aplysia. Science, 171(3974), 907-908.

[69] Wells, J., Kao, C., Mariappan, K., Albea, J., Jansen, E. D., Konrad, P., & Mahadevan-Jansen, A. (2005). Optical stimulation of neural tissue in vivo. Optics letters, 30(5), 504-506.

[70] Chernov, M., & Roe, A. W. (2014). Infrared neural stimulation: a new stimulation tool for central nervous system applications. Neurophotonics, 1(1), 011011.

[71] Shapiro, M. G., Priest, M. F., Siegel, P. H., & Bezanilla, F. (2013). Thermal mechanisms of millimeter wave stimulation of excitable cells. Biophysical journal, 104(12), 2622-2628.

[72] Richter, C. P., Matic, A. I., Wells, J. D., Jansen, E. D., & Walsh, J. T. (2011). Neural stimulation with optical radiation. Laser & photonics reviews, 5(1), 68-80.

[73] Ait Ouares, K., Beurrier, C., Canepari, M., Laverne, G., & Kuczewski, N. (2019). Opto nongenetics inhibition of neuronal firing. European Journal of Neuroscience, 49(1), 6-26.

[74] Christie, I. N., Wells, J. A., Southern, P., Marina, N., Kasparov, S., Gourine, A. V., & Lythgoe, M. F. (2013). fMRI response to blue light delivery in the naive brain: implications for combined optogenetic fMRI studies. Neuroimage, 66, 634-641.

[75] Stujenske, J. M., Spellman, T., & Gordon, J. A. (2015). Modeling the spatiotemporal dynamics of light and heat propagation for in vivo optogenetics. Cell reports, 12(3), 525-534.

[76] Thompson, S. M., Masukawa, L. M., & Prince, D. A. (1985). Temperature dependence of intrinsic membrane properties and synaptic potentials in hippocampal CA1 neurons in vitro. Journal of Neuroscience, 5(3), 817-824.

[77] Kim, J., & Connors, B. (2012). High temperatures alter physiological properties of pyramidal cells and inhibitory interneurons in hippocampus. Frontiers in cellular neuroscience, 6, 27.

[78] Volgushev, M., Vidyasagar, T. R., Chistiakova, M., & Eysel, U. T. (2000). Synaptic transmission in the neocortex during reversible cooling. Neuroscience, 98(1), 9-22.

[79] Talavera, K., Nilius, B., & Voets, T. (2008). Neuronal TRP channels: thermometers, pathfinders and life-savers. Trends in neurosciences, 31(6), 287-295.

[80] Albert, E. S., Bec, J. M., Desmadryl, G., Chekroud, K., Travo, C., Gaboyard, S., ... & Hamel, C. (2012). TRPV4 channels mediate the infrared laser-evoked response in sensory neurons. Journal of neurophysiology, 107(12), 3227-3234.

[81] Vincent, F., Acevedo, A., Nguyen, M. T., Dourado, M., DeFalco, J., Gustafson, A., ... & Duncton, M. A. (2009). Identification and characterization of novel TRPV4 modulators. Biochemical and biophysical research communications, 389(3), 490-494.

[82] Pedersen, S. F., & Nilius, B. (2007). Transient receptor potential channels in mechanosensing and cell volume regulation. In Methods in enzymology (Vol. 428, pp. 183-207). Academic Press.